Meningeal IL-17 producing T cells mediate cognitive impairment in salt-sensitive hypertension

Monica M. Santisteban[1]
Giuseppe Faraco[1]
David Brea Lopez[1]
Gang Wang[1]
Melissa Sobanko[1]
Rose Sciortino[1]
Gianfranco Racchumi[1]
Ari Waisman[2]
Josef Anrather[1]
Costantino Iadecola[1]

[1]Feil Family Brain and Mind Research Institute
Weill Cornell Medicine
New York, NY 10065, USA

[2]Institute for Molecular Medicine
University Medical Center,
Mainz, Germany

Correspondence:
Costantino Iadecola, MD
ORCID: 0000-0001-9797-073X
coi2001@med.cornell.edu

Monica M. Santisteban, PhD
ORCID: 0000-0002-2836-9075
mms2012@med.cornell.edu

Feil Family Brain and Mind Research Institute
Weill Cornell Medicine
407 E 61st Street
New York, NY 10065
Phone: 646-962-8279

Word Count:

Short running title: Meningeal IL-17 and cognitive impairment

NONSTANDARD ABBREVIATIONS

Ach: acetylcholine

Ang II: angiotensin II

ASL: arterial spin label

AT1R: ang II type 1 receptor

BAM: brain associated macrophages

bECKO: brain endothelial cell knockout

BM: bone marrow

BP: blood pressure

CBF: cerebral blood flow

DOCA: deoxycorticosterone acetate

eNOS: endothelial nitric oxide synthase

HTN: hypertension

i.c.v.: intracerebroventricular

IL-17: interleukin 17

IL-17RA: IL-17 receptor A

KO: knockout

NO: nitric oxide

RAS: renin angiotensin system

ROS: reactive oxygen species

Th17: T-helper 17

WT: wild-type

ABSTRACT

Hypertension, a disease afflicting over one billion individuals worldwide, is a leading cause of cognitive impairment, the mechanisms of which remain poorly understood. In a mouse model of hypertension involving brain angiotensin signaling, we found that the neurovascular and cognitive dysfunction depends on IL-17, a cytokine elevated in the circulation of hypertensive individuals. However, neither circulating IL-17 or brain angiotensin signaling could account in full for the dysfunction. Rather, IL-17 produced by meningeal T-cells was the major culprit by activating IL-17 receptors on brain associated macrophages. Accordingly, depleting brain macrophages or suppressing meningeal T cells completely rescued cognitive function without attenuating blood pressure elevation, circulating IL-17 or brain angiotensin signaling. The data unveil a critical role of meningeal T-cells and macrophage IL-17 signaling in the neurovascular and cognitive dysfunction of hypertension and suggest novel therapies to counteract the devastating effects of hypertension on cognitive health.

INTRODUCTION

Hypertension (HTN) is a major cause of death and disability worldwide, and a leading risk factor for dementia[1]. Although there have been significant advances in the pharmacotherapy, a sizable proportion of patients have uncontrolled or resistant HTN which is particularly damaging to the brain[2, 3]. Furthermore, despite suggestive evidence that a rigorous control of blood pressure (BP) may lower the risk of mild cognitive impairment[4], the burden of HTN on the brain remains substantial, including a 10% risk of recurrent cerebrovascular events despite BP control and no proven strategy to prevent dementia[5]. Therefore, there is need to gain a deeper understanding the damaging effects of HTN on the brain and to develop new approaches to protect cognitive health. Dysfunction of vital cerebrovascular regulatory mechanisms, such as the ability of neural activity to adjust the delivery of cerebral blood flow (CBF; functional hyperemia) or the regulation of microvascular perfusion by endothelial cells, have been strongly implicated in the deleterious effects of HTN on the brain[6]. However, the cellular and molecular basis through which the factors involved in BP elevation drive the neurovascular dysfunction associated with cognitive impairment remain poorly understood.

Salt-sensitivity is a critical factor in essential HTN[7], affecting approximately 50% of hypertensive individuals[8]. Experimental studies using the deoxycorticosterone acetate (DOCA)-salt model have provided evidence that the renin-angiotensin system (RAS) is activated in brain and suppressed in the periphery[9, 10]. Indeed, a large proportion of individuals with resistant HTN, particularly African American and women, exhibit low levels of circulating renin, a key protease needed for angiotensin II (Ang II) production, suggesting suppression of systemic RAS[11, 12]. It is also well established that HTN induces immune dysregulation and elevates circulating levels of the cytokine interleukin (IL)-17 both in animals and humans[13-17]. Interestingly, high dietary salt increases circulating levels of IL-17 by promoting polarization of T-helper 17 lymphocytes (Th17) in the gut, and induces neurovascular dysfunction and cognitive impairment[18-20].

However, the role IL-17 in the deleterious effects of salt-sensitive HTN on cognitive function, its sources and targets, and its relationships with brain RAS remain unexplored.

Here, we used the DOCA-salt model to examine the role of IL-17 in the neurovascular and cognitive dysfunction associated with salt-sensitive HTN. We found that DOCA-salt HTN alters key homeostatic mechanisms controlling the cerebral blood supply and leads to cognitive impairment. These deleterious effects are not driven by central Ang II signaling, but are associated with IL-17 signaling on both sides of the blood-brain barrier (BBB). In the circulation, IL-17 derived from gut and circulating T-cells activates IL-17 receptors A (IL-17RA) on cerebral endothelial cells to impair their ability to regulate cerebral perfusion, but this mechanism does not explain in full the cognitive deficits. On the brain side, unexpectedly, IL-17 derived from meningeal T-cells acts on IL-17RA on brain-associated macrophages (BAM)[21, 22] to induce neurovascular uncoupling and cognitive impairment. Accordingly, depletion of meningeal T-cells or BAM completely rescues the cognitive phenotype. These findings unveil a previously unappreciated critical involvement of meningeal T-cells and IL-17 in the cognitive impairment associated with salt sensitive HTN and suggest novel approaches to ameliorate the deleterious impact of HTN on cognitive function.

RESULTS

Salt-sensitive HTN induces neurovascular and cognitive impairment linked to expansion of gut IL-17-producing cells

First, we sought to examine the impact of salt-sensitive HTN on neurovascular and cognitive function. To this end, we used the DOCA-salt model of salt-sensitive HTN, in which mice are implanted with a s.c. pellet of DOCA and receive 0.9% NaCl in the drinking water[9, 23]. DOCA-salt treatment evoked a sustained elevation of BP beginning 3 days after pellet implantation (Fig 1A). An increase in circulating sodium was observed at 21 days (Suppl table 1), but the sodium content did not increase in brain, kidney and small intestine (Suppl Fig 1A). However, as

previously reported in mouse models and in individuals with refractory HTN[24], skin sodium content was increased without changes in potassium (Suppl Fig 1B). To examine the neurovascular effects of DOCA-salt HTN, we assessed CBF by laser-Doppler flowmetry in anesthetized mice with a cranial window overlying the somatosensory cortex under close monitoring of key physiological variables (Fig 1B; Methods)[25, 26]. DOCA-salt attenuated the increase in CBF evoked by neural activity induced by mechanical stimulation of the facial whiskers (functional hyperemia; Fig 1B-D), as well as the increase in CBF produced by bathing the somatosensory cortex with acetylcholine (ACh; Fig 1E), a response dependent on endothelial nitric oxide (NO)[27]. Both responses were impaired starting at day 10 after DOCA. However, smooth muscle vasoactivity, tested by neocortical application of adenosine (Fig 1F), BBB permeability to low molecular weight dextran (Suppl Fig 2A-B), and resting CBF (ml/100g/min) assessed by arterial spin label (ASL)-MRI (Suppl Fig 2C-D) were not impaired, indicating that the suppression of functional hyperemia and endothelial vasodilatation did not result from widespread neurovascular damage. DOCA-salt also altered cognitive function, as demonstrated by a reduction in the mice ability to discriminate between familiar and novel objects (working memory) (Fig 1G), a reduction of time spent in the target quadrant during the Barnes Maze probe trial (spatial learning and memory) (Fig 1H), and impaired nest building ability (activities of daily living) (Fig 1I). Importantly, the neurovascular alterations preceded the development of cognitive impairment (Fig 1D, E, G), an observation consistent with a mechanistic link between neurovascular dysfunction and cognitive impairment[6].

Based on the emerging role of IL-17 in human HTN[13-17] and in dietary salt-induced cognitive impairment[26], we then examined whether IL-17 contributes to the neurovascular and cognitive effects of DOCA-salt HTN. Circulating IL-17 increased gradually over the course of the DOCA-salt treatment (Fig 2A), beginning at day 10 when neurovascular dysfunction first became apparent (Fig 1D-E). Focusing on the gut, an organ enriched with IL-17-producing cells[28], we observed that DOCA-salt increased *Il17a* mRNA expression (Fig 2B). To identify the

cellular sources of IL-17, we induced DOCA-salt HTN in mice carrying the gene encoding eGFP at the *Il17a* locus[29] and observed increased IL17-GFP+ cells (Fig 2C) in the small intestine lamina propria, identified by flow cytometry to be Th17 and γδT17 cells (Fig 2DE-F). Th17 and γδT17 cells were also increased in blood and spleen (Fig 2G-H).

To test whether IL-17 contributes to the deleterious effects of salt-sensitive HTN, we induced DOCA-salt HTN in IL-17 deficient mice (IL17KO; Fig 2I, Suppl table 2). IL17KO mice developed an increase in BP and circulating sodium similar to wild-type (WT) mice (Suppl Fig 3, Suppl Table 1), but did not exhibit an attenuation in functional hyperemia and endothelial vasodilation (Fig 2J-K). Furthermore, no deficits were observed in either novel object or Barnes maze tests (Fig 2L-M). Thus, IL-17 produced by Th17 and γδT17 cells is essential for the neurovascular and cognitive dysfunction in DOCA-salt HTN.

<u>IL-17 impairs endothelial vasodilation by downregulating NO bioavailability via endothelial IL-17 receptors</u>

Next, we sought to identify the cellular targets of the IL-17 contributing to neurovascular and cognitive impairment. Since endothelial cells are in direct contact with circulating IL-17, which is elevated in DOCA salt HTN (Fig 2A), we first assessed the contribution of cerebral endothelial IL-17 receptors. To this end, we deleted brain endothelial IL-17RA by administering an adeno-associated virus expressing Cre recombinase in cerebral endothelial cells (AAV-BR1-iCre; i.v.)[30, 31] to IL-17RA$^{flox/flox}$ mice[32], referred to as IL-17RA^{bECKO}. AAV-BR1-iCre delivery in Ai14-ROSA^{tdTomato} reporter mice (Suppl Fig 4A) demonstrated 90-95% endothelial viral transduction in vessels less than 20μm, which includes the arterioles of interest (Suppl Fig 4B-D). Three weeks after AAV-BR1-iCre delivery we observed a reduction in *Il17ra* genomic DNA in sorted brain endothelial cells but not in microglia (Supp Fig 5), consistent with the selectivity of this viral vector[31, 33]. IL-17RA^{bECKO} mice (Fig. 3A) had increases in BP and circulating IL-17 comparable to

those of DOCA-salt WT mice (Suppl Fig 3, Suppl table 2), but the CBF response to ACh was completely rescued (Fig 3B). However, no improvement was observed in functional hyperemia (Fig 3C). Since the IL-17 has been shown to suppress endothelial NO production by inducing inhibitory eNOS phosphorylation at Thr^{495} [26], we also examined NO production and endothelial nitric oxide synthase (eNOS) phosphorylation in DOCA-salt treated mice. Resting and ACh-induced endothelial NO production was attenuated in DOCA cerebral microvascular preparations (Fig 3D), an effect associated with an increase in eNOS inhibitory phosphorylation (Fig 3E). However, as predicted by the rescue of endothelial vasoactivity (Fig 3B), the increase in eNOS Thr^{495} phosphorylation was suppressed in IL-$17RA^{bECKO}$ DOCA-salt mice (Fig 3F), attesting to the link between endothelial IL-17RA and eNOS inhibitory phosphorylation. Consistent with the partial rescue in neurovascular function, IL-$17RA^{bECKO}$ DOCA-salt mice displayed cognitive improvement only at novel object recognition, not the Barnes maze (Fig 3G-H).

<u>IL-17 impairs functional hyperemia via enhanced free radical production mediated by IL-17RA in BAM</u>

The partial neurovascular and cognitive rescue by cerebral endothelial IL-17RA knockdown suggests the involvement of IL-17RA on other vessel-associated cell types. BAM, including perivascular and leptomeningeal macrophages, express IL-17RA[34] and have been implicated in models of neurovascular and cognitive dysfunction[25, 35], raising the possibility that they may also play a role DOCA-salt HTN. To test this hypothesis, we examined the effect of BAM depletion via intracerebroventricular (i.c.v.) delivery of liposome-encapsulated clodronate (Fig 4A)[25, 35]. Liposomes containing vehicle (PBS) or clodronate were injected i.c.v. on the same day as DOCA-salt treatment was started. This protocol depletes 80% of perivascular and leptomeningeal macrophages (Fig 4B-C) within the time-frame of the experiment[25], without affecting microglia and blood leukocytes[25, 36]. The BP (Suppl Fig 3) and serum IL-17 (Suppl

table 2) increases evoked by DOCA-salt were not affected by clodronate treatment. However, BAM depletion completely normalized functional hyperemia (Fig 4D), and partially improved endothelial vasoactivity (Fig 4E). Additionally, BAM depletion improved cognitive function as assessed by novel object recognition and Barnes maze (Fig 4F-G).

Due to their myeloid origin, BAM are enriched with the ROS producing enzyme Nox2 and are major source of vascular oxidative stress[25, 37, 38]. Neocortical application of the ROS scavenger MnTBAP rescued the impairment of functional hyperemia in DOCA-salt (Fig 4H), attesting to the involvement of ROS in the neurovascular dysfunction. Therefore, we sought to determine if DOCA-salt increases ROS production in BAM and whether the effect is IL-17 dependent. Dissociated brain cells from WT control and DOCA-salt mice were incubated with the ROS probe dihydroethidium (DHE; Fig 4I) and stained for identification of BAM ($CD45^{hi}CD11b^{+}CD36^{+}$)[25, 39], microglia ($CD45^{int}CD11b^{+}$)[31, 40], and endothelial cells ($CD45^{-}Ly6C^{+}$)[31, 40] using flow cytometry (Suppl Fig 6A)[25, 31, 39, 40]. We found that DOCA-salt increased ROS production in BAM, but not in microglia or endothelial cells (Fig 4J). DOCA-salt failed to increase ROS in BAM of IL-17RA deficient mice (Fig 4K), indicating that IL-17 signaling is needed for BAM ROS production in DOCA-salt HTN. Consistent with this conclusion, recombinant IL-17 (10ng/mL) increased ROS production in BAM (Fig 4L).

The data presented above suggest that IL-17 acting on BAM contributes to the cerebrovascular and cognitive dysfunctions induced by DOCA-salt via IL-17. To provide further evidence that IL-17RA in BAM are involved, we used a bone marrow (BM) chimera-based approach. We and others have demonstrated that BM transplantation after total body irradiation repopulates leptomeningeal and perivascular compartments with BM-derived macrophages[25, 31, 41, 42]. Therefore, we transplanted $IL\text{-}17RA^{-/-}$ or $Nox2^{-/-}$ BM into WT mice to replace BAM with $IL\text{-}17RA^{-/-}$ or $Nox2^{-/-}$ BM-derived cells (Fig 4M). Three months later, mice were placed on the DOCA-salt protocol. WT mice transplanted with WT BM (WT→WT) exhibited alterations in CBF responses and cognition identical to those observed in naïve mice (Fig 4N-Q, Fig 1D-H),

indicating that although BAM in these mice are derived from the BM, they are pathogenically equivalent to native yolk sac-derived BAM[25, 35]. Deletion of either IL-17RA or Nox2 in BAM prevented the impairment of functional hyperemia in full (Fig 4N) and improved endothelial vasoactivity (Fig 4O), as observed in the BAM depletion experiments (Fig 4D-E). Additionally, IL-17RA$^{-/-}$→ WT and Nox2$^{-/-}$→ WT chimeras showed improved cognitive function (Fig 4P-Q). Attesting to the requirement of IL-17RA in BAM, ROS production was blunted in BAM from IL-17RA$^{-/-}$→ WT DOCA-salt chimeras (Suppl Fig 6B). Collectively, the findings with clodronate and BM chimera provide converging evidence that IL-17RA in BAM are critical for the alterations in functional hyperemia and cognitive function induced by DOCA-salt HTN.

Salt-sensitive HTN increases IL-17-producing T cells in the meninges

Next, we sought to define the cellular source(s) of IL-17 acting on BAM IL-17RA to induce neurovascular and cognitive dysfunction. Recent evidence indicates that IL-17-producing T cells are present in the meninges (dura mater)[43, 44], and are able to modulate rodent behavior[45, 46]. In agreement with these findings, *Il17a* mRNA was detected in stripped meninges of control mice and was markedly increased by DOCA-salt treatment (Fig 5A). *Il17a* mRNA was not observed in the brain parenchyma (Fig 5A). To map IL-17 producing cells in brain and meninges we used IL17-GFP reporter mice. Consistent with the mRNA data, IL17-GFP+ cells were not observed in the brain, but were found in the meninges (Fig 5B-D), as previously reported[45, 47]. DOCA-salt treatment led to a significant increase in IL17-GFP+ cells in the vicinity of the venous sinuses (Fig 5B). To determine whether these cells actually secrete IL-17, we performed an IL-17 ELISpot assay to detect cytokine release with single-cell resolution[48] in the isolated meningeal leukocytes. We found that meningeal cells secrete IL-17, and this response is increased in DOCA-salt mice (Fig 5E-F). We then used flow cytometry to characterize the IL17-GFP+ cells. We found an increase in the percentage of γδT17 cells but no difference in Th17 cells (Fig 5G-K), suggesting that meningeal T-cells could be source of the IL-17 acting on BAM IL-17RA to

induce neurovascular and cognitive dysfunction. We did not observe changes in key inflammatory genes (Suppl Fig 7A-B) or evidence of microglia and astrocyte activation (Suppl Fig 7C-D), suggesting that meningeal IL17 did not result in a massive neuroinflammatory reaction which could potentially contribute to cognitive impairment In DOCA-salt.

Cognitive impairment in salt-sensitive HTN is driven by meningeal IL17-producing T cells

Next, we sought to provide evidence in support of the involvement of meningeal IL17-producing cells in the neurovascular and cognitive effects of DOCA salt HTN. Meningeal γδT cells, like other γδT cells[49], are tissue resident, with only 1-2% being derived from the circulation under homeostasis[45]. However, in inflammatory conditions, an increased influx of γδT cells into lymph nodes and subsequent homing to inflamed tissues via the circulation has been shown[50, 51]. Given that circulating Th17 and γδT17 cells are both elevated in DOCA-salt, it is conceivable that T cells migrate from the circulation to the meninges. To test this hypothesis, we utilized FTY720 (fingolimod), a sphingosine-1-phosphate receptor modulator that depletes circulating lymphocytes by preventing their egress from lymphoid tissues and other mechanisms[52-55]. FTY720 (1mg/kg i.p. every 3 days[26]) was administered from day 7 through day 21 of DOCA-salt treatment (Fig 6A) and did not affect the development of HTN (Fig 6B). As expected, FTY720 significantly reduced circulating $CD4^+$ T cells (Fig 6C) without affecting the elevation in serum IL-17 in DOCA-salt mice (Fig 6D). FTY720 depleted IL17-GFP+ cells in the meninges (Fig 6E), with a near complete depletion of Th17 cells (Fig 6F), and a 66% reduction in γδT17 cells (Fig 6G). Interestingly, FTY720 did not ameliorate the CBF response evoked from the endothelium (Fig 6H), attesting to its dependence on circulating IL-17 acting on cerebral endothelial IL-17RA and not BAM. The reduction of IL-17 producing T cells in the meninges was associated with full rescue of functional hyperemia (Fig 6I) and improved of cognitive function (Fig 6J-K), as well as suppression of ROS production in BAM (Suppl Fig 6C). Thus, meningeal IL17-producing T-cells

are the source of the IL-17 contributing to the neurovascular and cognitive impairment in salt-sensitive HTN.

The contribution of Ang II to the cerebrovascular dysfunction in DOCA-salt depends on IL-17 signaling

It is well established that the DOCA-salt treatment leads to activation of brain RAS[9, 10], which has been implicated in endothelial dysfunction in large and small cerebral vessels[56]. In apparent contrast, our data suggest that IL-17 is essential for the neurovascular and cognitive dysfunction in DOCA-salt HTN. Therefore, we investigated the relationship between brain Ang II and IL-17 in this model. As expected, DOCA-salt treatment elevated Ang II levels in brain and reduced it in the circulation (Fig 7A-B). These effects were associated with mRNA upregulation of brain Ang II receptors type 1A (AT1R) (*Agtr1a*; Fig 7C*)* and downregulation of kidney renin (*Ren1*; Fig 7D), consistent with activation of RAS in brain and suppression in the periphery[56]. Central AT1R blockade by i.c.v. infusion of losartan (Fig 7E), prevented the increase in BP caused by DOCA-salt[9] (Suppl Fig 3) but did not attenuate the increase in circulating IL-17 (Suppl table 2). Accordingly, i.c.v. losartan restored functional hyperemia (Fig 7F), but did not improve endothelium-dependent vasodilation (Fig 7G) consistent with circulating IL-17 being the predominant mediator of the endothelial dysfunction. Central AT1R blockade ameliorated cognitive impairment only partially, with an improvement observed only in novel object recognition, but not at the Barnes maze (Fig 7H-I). Since Ang II induces ROS production in BAM leading to neurovascular dysfunction[25], we wondered if IL-17 signaling in BAM is required for Ang II-induced ROS production. Ang II stimulation increased ROS production in WT but not IL17RA$^{-/-}$ BAM (Fig 7J). However, indices of brain RAS activation were not attenuated in IL17KO mice (Suppl Fig 8A) or mice in which meningeal production of IL-17 was suppressed by treatment with FTY720 (Suppl Fig 8B), suggesting that brain RAS activation in the absence of meningeal IL-17 is not sufficient to induce neurovascular dysfunction. In support of this

conclusion, bathing the cerebral cortex with Ang II to activate AT1R on BAM[25], induced neurovascular dysfunction in WT but not IL17KO mice (Fig 7K-L). Thus, IL-17 signaling is necessary for the contribution of Ang II to the neurovascular and cognitive impairment of salt-sensitive HTN.

DISCUSSION

We have demonstrated that the neurovascular and cognitive dysfunction associated with salt-sensitive HTN is mediated by IL-17 signaling in cerebral endothelium and BAM. In the circulation, IL-17 produced mainly by T-cells located in the gut acts on cerebral endothelial IL-17RA to reduce NO production leading to suppression of endothelial vasoactivity without affecting the increase in CBF induced by neural activity. In the brain, IL-17 produced by meningeal T-cells acts on IL-17RA on BAM to induce vascular oxidative stress and suppression of functional hyperemia with minimal effects on endothelial function. However, these two mechanisms do not contribute equally to the cognitive dysfunction: counteracting the effect of circulating IL-17 by endothelial IL-17RA deletion rescues cognition only partially, while counteracting the sources (T-cells) or targets of central IL-17 (BAM or BAM IL-17RA) rescues cognitive function in full. Therefore, the data unveils an unanticipated central role of meningeal T-cells in the deleterious cognitive effect of salt sensitive hypertension.

There is increasing evidence that inflammation and immunity participate in the pathobiology of HTN[57]. Pioneering studies have unveiled a role of innate and adaptive immunity in the central and peripheral mechanisms driving the elevation in BP and on the end organ damage, particularly in the kidney and the vasculature[58-60]. In this context, T-cells and IL-17 have emerged as important mediators of the effect of Ang II and DOCA-salt HTN on peripheral organs and vessels, in part verified in hypertensive patients[61]. Here, we extend these observations by providing evidence that meningeal T-cells and IL-17 play a critical role in the neurovascular and cognitive deficits in a model of HTN reproducing key attributes of the human

disease[10, 62]. While the meninges have recently been recognized as major players in the immune responses of the brain underling brain injury and repair[43, 45], our findings provide insight into an unanticipated pathogenic role of meningeal immunity. Our studies revealed that the meninges are the critical site of the immune responses underlying the cognitive deficits in HTN. This process is driven by a cross-talk between meningeal T-cells and BAM through IL-17 signaling. Thus, depletion of IL-17-producing T-cells in the meninges, depletion of BAM or deletion of IL-17RA on BAM, rescues the cognitive deficits in full.

The DOCA salt model is associated with increases in brain RAS signaling and reduction of the systemic RAS[10], which we have verified by central and peripheral measurements of Ang II. DOCA salt HTN is well established to induce alterations in cerebral vascular regulation both in vivo and in isolated cerebral arteries and arterioles[23, 56]. Surprisingly, however, our study showed that the vascular effects of Ang II, mediated by ROS production by BAM, require IL-17. Thus, ex vivo Ang II is unable to increase ROS production in BAM in the absence of IL-17RA, and in vivo Ang II applied to the neocortex to target meningeal and perivascular BAM does not induce neurovascular dysfunction IL17KO mice. These observations unveil a critical requirement of meningeal IL-17 in the deleterious effects of Ang II. Considering the key role that Ang II and IL-17 signaling play in health and disease the molecular bases of their interaction is of great interest and will require further exploration.

Owing to the absolute reliance of the brain on the delivery of blood flow, reduced cerebral perfusion or alterations in neurovascular regulation have long been implicated in cognitive impairment induced by vascular factors as well as Alzheimer's disease[63, 64]. Our studies, in general, support a link between CBF regulation and cognitive health, but they also suggest effects of IL-17 independent of blood flow. While resting CBF is not reduced, blocking cerebral endothelial IL-17 signaling rescues endothelial vasoactivity and produces partial cognitive improvement. On the other hand, counteracting central Ang II signaling rescues only neurovascular coupling and leads to a partial improvement in cognition. These data would

suggest an additive role of endothelial dysfunction and neurovascular uncoupling in the cognitive deficits. However, this possibility is unlikely because depletion of meningeal T-cells provides complete cognitive rescue while improving only neurovascular coupling and not endothelial function. These data suggest alternative roles of IL-17 signaling in inducing cognitive dysfunction, such as direct effects on IL-17 on neurons as demonstrated in other models[45, 46, 65, 66].

It is well established that HTN is a leading risk factor for cognitive impairment caused both by vascular factors and neurodegeneration[6], but the evidence that antihypertensive therapy reduces such risk is inconsistent and limited[67, 68]. Our findings reveal an additional layer of complexity in the deleterious effects of HTN on the brain and suggest new preventive and therapeutic approaches. The central actions of Ang II are critical for the development of HTN by inducing neurohumoral dysfunction. This aspect was highlighted by our observation that central inhibition of AT1R prevented the BP elevation completely but did not rescue the cognitive dysfunction in full. While BP control remains critical for attenuating hypertensive end-organ damage to kidney, heart, and vasculature[69], full protection of the brain may require also targeting meningeal immunity. Considering the diversity of mechanisms underlying human HTN[70], efforts to select hypertensive patients in which immune factors are involved, may identify individuals at greater risk for the deleterious effects of meningeal immune signaling on the brain. Since the infectious complications of suppressing immune signaling is a well-known concern in patients with cardiovascular diseases[71], strategies to selectively target meningeal immunity would be required[72].

MATERIALS AND METHODS

The data that support the findings of this study are available from the corresponding authors upon request. Details on antibodies used and specific primer sequences are found in the Online Supplement.

Mice and General surgical procedures

All procedures were approved by the Institutional Animal Care and Use Committee of Weill Cornell Medicine and performed in accordance with the National Institutes of Health (NIH) Guide for the Care and Use of Laboratory Animals. Studies were performed in a blinded fashion in male C57BL/6 mice (WT, age 3-5 months, weight 25-30g; JAX, the Jackson Laboratory), IL-17 GFP reporter mice (C57BL/6-*IL17a*^{tm1Bcgen}/J, JAX strain# 018472), IL-17 knockout mice (*IL17a*$^{tm1.1(icre)Stck}$/J, JAX strain# 016879), and IL-17RA$^{flox/flox}$ mice[32]. IL-17RA$^{flox/flox}$ mice were crossed with the germ-cell driven Sox2-Cre mice (B6.Cg-*Edil3*$^{Tg(Sox2-cre)1Amc}$/J, JAX strain# 008454)[73] to generate whole-body IL-17RA knockout mice. Bone marrow chimera experiments detailed below were performed on C57BL/6 mice receiving donor cells from IL-17RA knockout mice or B6.129S-*Cybb*^{tm1Din}/J mice (*Nox2*$^{-/-}$, JAX strain# 002365), both lines are congenic for C57BL/6. AAV-BR1-iCre experiments detailed below were performed on B6.Cg-*Gt(ROSA)26Sor*$^{tm14(CAG-tdTomato)Hze}$/J (Ai14 TdTomato reporter, JAX strain# 007914), and homozygous IL-17RA$^{flox/flox}$ mice. Female mice were not included in this study, as previous studies have shown that they have a blunted hypertensive and immune response to DOCA-salt[74].

DOCA-salt HTN

Mice were randomized to treatment group and anesthetized by isoflurane inhalation for subcutaneous implantation of a 50 mg pellet of DOCA (Innovative Research of America, Cat# M-121) or sham surgery of equal duration[23]. After recovery from anesthesia, DOCA animals were maintained on standard chow and *ad libitum* access to 0.9% NaCl in autoclaved tap water. Control animals were maintained on standard chow and *ad libitum* access to autoclaved tap water. Systolic BP was monitored in awake mice using tail-cuff plethysmography (Hatteras)[25, 31].

Mice were acclimated to tail-cuff plethysmography for one week prior to pellet or sham surgery, and systolic BP was monitored twice a week after initiation of DOCA-salt.

Tissue sodium measurement

Mice were anesthetized with isoflurane, and blood was collected through cardiac puncture. Brain, kidney, skin (dorsal abdomen), and distal small intestine (distal 10 cm) were isolated, flash frozen, and stored at -80°C until analysis. After 15 minutes, blood was centrifuged at 2,000*g* for 15 minutes and serum was separated and stored at -80°C until analysis. The serum renal chemical panel was performed by the Laboratory of Comparative Pathology (LCP) of Weill Cornell Medicine Research Animal Resource Center, and the tissue mineral panel for sodium measurement was performed by the Animal Health Diagnostic Center Toxicology Lab of Cornell University Veterinary Medicine using inductively coupled plasma – atomic emission spectrometry (ICP-AES)[75, 76].

General surgical procedures for CBF studies

Mice were anesthetized with isoflurane (induction, 5%; maintenance, 2%) and artificially ventilated with a mixture of N_2 and O_2. One of the femoral arteries was cannulated for recording mean arterial pressure (MAP) and collecting blood samples. Rectal temperature was maintained at 37°C. After surgery, isoflurane was discontinued and anesthesia was maintained with urethane (750 mg/kg, i.p.) and chloralose (50 mg/kg, i.p.). Throughout the experiment, the level of anesthesia was monitored by testing of motor responses to tail pinch. Arterial blood gases were monitored at the beginning and end of the experiment and maintained at pO_2 100-110mmHg, pCO2 30-40mmHg, and pH 7.3-7.4[25]. As in previous studies[77], MAP remained within the autoregulated range for CBF (Control: 82.77 ± 0.85 mmHg; DOCA: 106.37 ± 0.99 mmHg;

p<0.05). Due to the anesthesia, the baseline BP and the increase in BP induced by DOCA-salt was lower than that observed in awake mice[9].

Experimental protocol for experiments monitoring CBF reactivity

As previously performed[25, 26, 35], a small craniotomy (2 × 2 mm) was performed to expose the parietal cortex, the dura was removed, and the site was superfused with Ringer's solution (37°C; pH 7.3–7.4)[25]. CBF was continuously monitored at the site of superfusion with a laser-Doppler probe (Perimed) positioned stereotaxically on the cortical surface and connected to a data acquisition system (PowerLab). CBF values were expressed as percentage increases relative to the resting level. After MAP and blood gases were stable, CBF responses were recorded. The whisker-barrel cortex was activated for 60 seconds by stroking of the contralateral vibrissae, and the evoked changes in CBF were recorded. ACh (10 μM; Sigma-Aldrich) or adenosine (400 μM; Sigma-Aldrich) was superfused on the exposed neocortex for 5 minutes[25, 26, 35]. In some experiments, CBF responses were tested before and after 30 minutes of superfusion with the ROS scavenger MnTBAP (100μM)[25, 77] or Ang II (500nM)[25, 78].

Measurement of resting CBF by ASL-MRI

CBF was assessed quantitatively using arterial spin labeling magnetic resonance imaging (ASL-MRI), performed on a 7.0-tesla 70/30 Bruker Biospec small-animal MRI system with 450 mT/m gradient amplitude and a 4,500 $T \cdot m^{-1} \cdot s^{-1}$ slew rate. A volume coil was used for transmission and a surface coil for reception. Anatomical localizer images were acquired to find the transversal slice approximately corresponding to bregma +0.5 mm. This position was used for subsequent ASL-MRI, which was based on a flow-sensitive alternating inversion recovery rapid acquisition with relaxation enhancement (FAIR-RARE) pulse sequence labeling the inflowing blood by global inversion of the equilibrium magnetization. One axial slice was acquired with a field of view of 15 × 15 mm, spatial resolution of 0.117 × 0.117 × 1 mm, TE (echo time) of

5.368 ms, effective TE of 48.32 ms, recovery time of 10 s, and a RARE (rapid imaging with refocused echoes) factor of 72. Twenty-two turbo inversion recovery values ranging from 30 to 2,300 ms were used, and the inversion slab thickness was 4 mm. For computation of resting CBF (rCBF), the Bruker ASL perfusion processing macro was used. It uses a published model[79] and includes steps to mask out the background. The masked rCBF images were exported to Analyze format on the MRI console. The ASL images were analyzed by ImageJ and the average CBF value is reported in mL per 100 g of tissue per min[26].

BBB permeability

BBB permeability was assessed using fluorescein-dextran (FITC-dextran, MW 3 kDa; 100µl of 1% solution i.v.), as previously described[25, 31]. The tracer was allowed to circulate for 20 minutes, and then mice were transcardially perfused with cold PBS to clear the intravascular tracer. Brains were removed and olfactory bulb, brainstem, and cerebellum were discarded. Samples were weighed and frozen on dry ice and stored at −80 °C until analysis. Tissue was homogenized in 400µL of PBS, mixed with 400µL of methanol, and centrifuged at 13,000*g* for 30 minutes. The supernatant was used for measurement of the amount of FITC-dextran (485nm excitation and 530 nm emission), measured in duplicate using a fluorescence spectrophotometer, together with standards, and normalized to brain tissue weight.

Novel object recognition test

The novel object recognition test (NOR) task was conducted in a plastic box measuring 29 cm × 47 cm × 30 cm high[25, 26]. Stimuli consisted of plastic objects that varied in color and shape, but had similar size. A video camera was used to record the testing session for offline analysis using AnyMaze software. Mice were acclimated to the testing room for 1 hour each day prior to the start of each day. On day 1, mice were acclimated to the testing chamber (habituation). On day 2, mice were placed in the same chamber in the presence of 2 identical sample objects and

were allowed to explore for 5 minutes. After an intersession interval of 1 hour, mice were placed in the same chamber, but 1 of the 2 objects was replaced by a novel object. Mice were allowed to explore for 5 minutes. Between trials, the maze is cleaned with 10% ethanol in water to minimize olfactory cues. Exploratory behavior was assessed manually by two experimenters blinded to the treatment group. Exploration of an object was defined as the mouse sniffing the object or touching the object while looking at it[25]. A minimal exploration time for both objects (total exploration time) during the test phase (5 seconds) was used. The amount of time taken to explore the novel object was expressed as percentage of the total exploration time and provides an index of working memory.

Barnes Maze

As described previously[25, 26], we used a Barnes maze consisting of a circular open surface (90 cm in diameter) elevated to 90cm by four wooden legs. There are 20 circular holes (5 cm in diameter) equally spaced around the perimeter, positioned 2.5cm from the edge of the maze. No wall or intra-maze visual cues are placed around the edge. A plastic escape box (11 x 6 x 5 cm) was positioned beneath one of the holes. Mouse movement is tracked with the Any-Maze software (Stoelting). Mice are tested in groups of 10, and between trials are placed into cages in a dark room adjacent to the test room for the intertrial interval (45 minutes). Mice are habituated to the dark room for 60 min prior to the start of each day. No habituation trial is performed. The acquisition phase consists of three consecutive training days with three 3-minute trials per day with the escape hole located at the same location across trials and days. On each trial, a mouse is placed into a start tube located in the center of the maze, the start tube is raised, and the buzzer is turned on until the mouse enters the escape hole. After each trial, mice remain in the escape box for 60s before being returned to their home cage. Between trials, the maze is cleaned with 10% ethanol in water to minimize olfactory cues. Three parameters of learning performance are recorded: (1) latency to locate the escape hole, (2) distance traveled before

locating the escape hole, and (3) number of errors made. Errors are defined as head-pokes into non-escape holes and are counted manually. On the fourth day, the probe trial is performed and consists of a 1.5 min trial where the escape hole has been removed. The memory parameter recorded is percent of time spent in the target quadrant where the escape hole used to be.

Nest building

The ability of mice to build nests is assessed by the Deacon rating scale[26, 80]. 1 hour prior to the dark cycle, each mouse is placed in a new clean cage containing 5g of nestlet (Ancare) in the middle of the cage. Food, water, and lighting parameters are not changed from standard housing practices. The next day, nests are assessed on a rating scale of 1-5[80], and untorn nestlet pieces are weight. The cognitive parameters recorded are (1) nest score, and (2) percent of untorn nestlet.

IL-17 measurement

IL-17 concentration in serum was measured by cytometric bead array mouse IL-17A Enhanced Sensitivity Flex Set (BDBiosciences)[26] or by electrochemiluminescence-based multi-array MSD V-Plex Mouse IL-17A Kit (MesoScale)[81], according to the manufacturer's instructions.

Immunofluorescence

IL17-eGFP and wild-type mice were anesthetized with sodium pentobarbital (120 mg/kg, i.p.) and perfused transcardially with phosphate-buffered saline (PBS) followed by 4% paraformaldehyde (PFA) in PBS. Distal small intestine, brain, and skull cap were removed and post-fixed overnight in 4% PFA. Small intestine was then submerged in 30% sucrose solution for 3 days, frozen, and sections (thickness: 30 µm) were cut through the whole distal small intestine using a cryostat and then place on a slide. Coronal brain sections (thickness 40 µm) were cut through the whole brain using a microtome. Sections were permeabilized in 0.5%

Triton-PBS and then blocked with 5% of normal donkey or goat serum in 0.1% Triton-PBS. Sections were incubated with primary antibodies (Suppl Table 3) at 4°C overnight in 2% normal donkey or goat serum in 0.1% Triton-PBS. Sections were then incubated with a secondary antibody (Suppl Table 4) and mounted on slides with VectaShield Hardset mounting medium with DAPI (Vector Labs), visualized with a laser-scanning confocal microscope (Leica TCS SP8), and analyzed on ImageJ software by an investigator blinded to the treatment groups.

Cell suspension preparation from lymph nodes, spleen, and blood

At the indicated timepoints, mesenteric, axillary and inguinal lymph nodes were extracted, placed on a premoistened 70-μm cell strainer, gently triturated, washed with 10 mL of PBS and spun at 500*g* for 7 min[26]. The cell suspension was then either stained for flow cytometry analysis or processed for analysis of intracellular cytokines. The spleen was removed, its epithelium was cut longitudinally, and cells were isolated as described for the lymph nodes. Blood (150 μL) was drained from the submandibular venous plexus into heparinized tubes, incubated with erythrocytes lysis buffer and spun at 500*g* for 7 min, and cells were stained for flow cytometry analysis[26].

Isolation of intestinal lamina propria mononuclear cells

Mice were euthanized by isoflurane overdose, and small intestines were removed and separated as previously described[26, 29]. Peyer patches were cut out from the small intestine and small intestines were completely cleaned of mesenteric fat and intestinal contents[26]. Then intestines were opened longitudinally, washed of fecal contents with PBS, cut into approximately 1 cm pieces and placed into 20 mL of HBSS/10 mM HEPES, 8% FBS, 4 mM EDTA, 0.5 mM DTT. Next intestinal pieces were washed three times in a shaking incubator set at 250 rpm and at 37 °C for 20 min. After each round, intestinal pieces were vortexed for 20 s and the cell suspension containing intraepithelial lymphocytes (IELs) was collected. Suspensions from the

three washes of IELs were combined and filtered over 0.3 g of prewashed nylon wool placed into a 10-mL syringe and then over a 70-μm strainer. Intestinal pieces were washed with complete PBS to remove EDTA, minced thoroughly with scissors and placed into 5 mL of 0.2 mg/mL of collagenase D in HBSS/10 mM HEPES with 5% of FBS. Then the intestinal pieces were digested at 250 rpm and 37 °C for 20 min, followed by 20 s of vortex. The resulting cell suspension contained the LPMCs, and was filtered with a 40-μm nylon cell strainer; the strainer was washed with 10 mL of PBS. LPMCs cell suspensions were spun at 500*g* for 10 min at 4 °C. Cell pellets were resuspended in 8 mL 44% Percoll and overlaid on 5 mL of 67% Percoll. Gradients were centrifuged at 500*g* for 20 min at 4 °C (without brake) and cells at the interface were collected and washed with 10 mL of PBS. Cells were then spun at 500*g* for 10 min at 4 °C and cells were stained for flow cytometry analysis.

Isolation of brain and meningeal leukocytes

Isolation of brain leukocytes was performed as described[31]. Mice were anesthetized with pentobarbital (100 mg/kg, i.p.) and transcardially perfused with heparinized PBS. Brain cell isolation was performed by enzymatic digestion with Liberase DH (Roche Diagnostics) and Dispase (Worthington). Brain hemispheres were separated from the cerebellum and olfactory bulb and gently triturated in HEPES-HBSS buffer containing the following: 138mM NaCl, 5mM KCl, 0.4mM Na_2HPO_4, 0.4mM KH_2PO_4, 5mM d-glucose, and 10mM HEPES using a Gentle MACS dissociator (Miltenyi Biotec) following the manufacturer's instructions. The meninges were stripped following removal of the brain from the skull[82], leaving the pia mater attached to the brain surface, using a dissection microscope. The suspension was digested with 125 μg/ml Liberase, 0.8U/ml dispase, and 50 U/ml DNase I at 37°C for 45 min (brain) or 15 min (meninges) in an orbital shaker at 100 rpm. Brain cells isolated were washed and subjected to 30% Percoll (GE Healthcare) density gradient centrifugation at 500*g* for 15 min. Meninges were placed on the surface of a premoistened 70-μm cell strainer. Tissue was gently homogenized

with the end of a 1-mL syringe plunger, washed with 20 mL 2% FBS in PBS and centrifuged at 500*g* for 7 min.

ROS assessment by flow cytometry

Following isolation of brain leukocytes, cells were incubated with dihydroethidium (DHE, 2.5μM) in stimulation buffer (RPMI-1640, 10% (v/v) heat inactivated FBS, 100 units/mL penicillin, 100 μg/mL streptomycin) for 30 minutes at 37° and 5% CO_2. Some cells were pooled and separated for stimulation experiments, and were incubated with PBS, murine recombinant IL-17 (10ng/mL, Preprotech), or Ang II (300nM, Sigma) for 30 minutes prior to addition of DHE (as above). Cells were washed with FACS buffer (1X PBS, 2% FBS, 0.05% NaN_3) and centrifuged at 500*g* for 7 min.

Flow cytometry and fluorescence activated cell sorting

For surface marker analysis, 1×10^6 cells approximately were resuspended in 50 μL of FACS buffer. Cells were blocked with anti-CD16/CD32 for 10 min at 4 °C and then stained with the appropriate antibodies for 15 minutes at 4 °C. Antibodies and concentrations used are listed in Supplementary table 4. Cells were washed with FACS buffer, resuspended in 200 μL of FACS buffer and acquired NovoSampler Q (NovoCyte Quanteon), and absolute cell numbers and frequencies were recorded. Samples were analyzed with FlowJo (Vers.10, Tree Star) by an investigator blinded to the treatment groups (Suppl Figs 6 and 9). Appropriate isotype controls, "fluorescence minus one" staining, and staining of negative populations were used to establish sorting parameters. Endothelial cells were identified as $CD45^-Ly6C^+$, microglia were identified as $CD45^{int}CD11b^{+}$[31], and brain macrophages were identified as $CD45^{hi}CD11b^{+}CD36^{+}$[39]. For fluorescence activated cell sorting, endothelial and microglia cells (Suppl Fig 5) were sorted on

a FACSAria II (BD Biosciences) or CytoFlex SRT (Beckman) and collected in sample buffer for genomic DNA qRT-PCR.

Nitric oxide measurement in pial microvessels

Pial microvessels were removed under a dissecting microscope[83] and incubated with DAF-FM (25 μM; Molecular Probes) in l-ACSF (124 mM NaCl, 26 mM $NaHCO_3$, 5 mM KCl, 1 mM NaH_2PO_4, 2 mM $CaCl_2$, 2 mM $MgSO_4$, 20 mM glucose, 4.5 mM lactic acid, oxygenated with 95% O_2 and 5% CO2, pH=7.4) at room temperature for 45 min[26, 83]. Time-resolved fluorescence was measured every 60 s with an exposure time of 150 ms using image analysis software (IPLab, Scanalytics Inc). After a stable fluorescence baseline was achieved, microvessels were superfused with ACh (100 μM) for 15 min. DAF-FM fluorescence intensity is expressed as RFU/μm^2, where RFU is the relative fluorescence unit, and μm^2 is unit of the area in which RFU was measured.

Western blotting

Cerebral blood vessels and brain microvascular endothelial cells samples were lysed in RIPA buffer (50 mM Tris-HCl pH 8.0, 150 mM NaCl, 0.5% deoxycholic acid, 0.1% SDS, 1 mM EDTA pH 8.0, 1% IGEPAL CA-630) and equal volumes were mixed with SDS sample buffer, boiled, and analyzed on 4–12% SDS polyacrylamide gels. Proteins were transferred to PVDF membranes (Millipore), blocked with 5% milk in TBS/0.1% Tween-20 (TBST) and incubated with anti-phospho-eNOS (Thr^{495}) and anti-eNOS (Suppl Table 4; 1:1,000, Cell Signaling cat. #9574 and 9572, respectively). Membranes were washed in TBST, incubated with goat anti-rabbit secondary antibodies conjugated to horseradish peroxidase (Suppl Table 4, Santa Cruz Biotechnology), and protein bands were visualized with Clarity Western ECL Substrate (Bio-Rad) on a Bio-Rad ChemiDoc MP Imaging System.

Cerebral endothelial knockdown of IL17-RA

Seven-ten week-old C57BL/6J, B6.Cg-*Gt(ROSA)26Sor*$^{tm14(CAG-tdTomato)Hze}$/J (Ai14 TdTomato reporter, Stock #007909), and IL-17RA$^{flox/flox}$ mice[32] mice were administered 1.8x10^{11} VG in 100µL sterile PBS of AAV-BR1-iCre[30, 31] (AAV-NRGTEWD-CAG-iCre). DOCA pellets were implanted three weeks after AAV-BR1-iCre administration.

In vivo treatments

To deplete cerebral CD206^{+} brain macrophages, clodronate- or PBS-loaded liposomes were prepared as previously described[25, 31]. Under isoflurane anesthesia, 10 µl of clodronate-liposomes (7 mg/ml) and PBS-liposomes (vehicle) were injected (500 nl/min) into the cerebral ventricles (i.c.v.) with a Hamilton syringe through a burr hole drilled on the right parietal bone (coordinates: 0.5 mm posterior to bregma 1.0 mm lateral from midline, 2.3 mm below the brain surface) on the same day as DOCA pellet implantation. FTY720 (1 mg/kg; Cayman Chemical)[26] was injected i.p. three times every 3 d after the first week of DOCA-salt. Control and DOCA-salt mice were equipped with an intracerebroventricular (i.c.v.) cannula attached to a osmotic mini-pump (ALZET brain infusion kit 3 #0008851, pump #1004) for delivery of losartan (5µg/hour) or saline on the same day as DOCA pellet implantation.

qRT-PCR

Procedures for RT-PCR were identical to those previously described[25, 26, 31]. Briefly, samples were collected in TRIzol (Invitrogen Life Technologies) and RNA was extracted according to the manufacturer's instructions. RNA samples were treated with Rnase-free DnaseI (Roche) to remove DNA contamination. cDNA was produced from mRNA samples using the RevertAid First Strand cDNA Synthesis Kit (Thermo Scientific). Quantitative determination of gene expression was performed on a Chromo 4 Detector (Bio-Rad, Hercules, CA) using a two-step cycling protocol. Hypoxanthine-guanine phosphoribosyltransferase (HPRT) was used to

normalize gene expression. qRT-PCR was conducted with cDNA in duplicate 15-µL reactions using the Maxim a SYBR Green/ROX qPCR Master Mix (2×) (Thermo Scientific). The reactions were incubated at 50°C for 2 min and then at 95°C for 10 min. A polymerase chain reaction cycling protocol consisting of 15 s at 95°C and 1 min at 60°C for 45 cycles was used for quantification. Relative expression levels were calculated according to Livak and Schmittgen, and values were normalized to respective normal control samples. Reference primer sequences are described in Suppl table 4.

For assessment of *Il17ra* knockdown *in vivo*, genomic DNA was extracted from sorted endothelial and microglia cells. Cre recombination specifically targets exons 4-7 of the *Il17ra* gene in IL17-RA$^{flox/flox}$ mice, thus we normalized *Il17ra* exon 5 expression to the non-targeted *Il17ra* exon 3. Primer sequences as described in Suppl table 4.

Bone marrow transplant

As previously described[25, 31], whole-body irradiation was performed on 6-week-old C57BL/6 male mice with a lethal dose of 9.5 Gy of γ radiation using a ^{137}Cs source (Nordion Gammacell 40 Exactor). Eighteen hours later, BM cells (2 × 10^6, i.v.) isolated from donor IL-17RA knockout mice or B6.129S-*Cybb*^{tm1Din}/J mice (*Nox2*$^{-/-}$, JAX stock# 002365) were transplanted in irradiated mice. Mice with transplanted BM cells were housed in cages with Sulfatrim diet for the first 2 weeks.

BBB permeability measurement

BBB permeability was assessed using fluorescein-dextran (FITC-dextran, MW 3 kDa; 100µl of 1% solution i.v.), as previously described[25, 26, 31]. The amount of FITC-dextran (485nm excitation and 530 nm emission) was determined in duplicate using a fluorescence spectrophotometer, together with standards, and normalized to brain tissue weight.

IL-17A ELISpot Assay

Meningeal leukocytes were isolated as described above, and incubated in ELISpot plate for 4 hours in stimulation buffer (RPMI-1640, 10% (v/v) heat inactivated FBS, 100 units/mL penicillin, 100 µg/mL streptomycin, 100 ng/mL phorbol 12-myristate 13-acetate (PMA), 1 µg/mL of ionomycin) in a 37C humidified incubator with 5% CO2. Mouse IL-17A ELISpotPLUS kit ALP (MABTECH, Cat# 3521-4APW-2) was performed following manufacturer's instructions. Wells were developed with BCIP/NBT-plus for 15 minutes, and color development was stopped by washing with diH2O. Images were obtained using a digital camera (T TAKMLY, MX200-B) and analyzed using ImageJ software.

Ang II assay

Mice were euthanized, and blood was collected by cardiac puncture in a prechilled tube containing a mix of protease inhibitors. Plasma was collected and transferred to a prechilled tube and stored frozen at –80°C. Brains were collected and immediately frozen on dry ice. Ang II concentration was determined using a radioimmunoassay by the Hypertension Core Laboratory of the Wake Forest University School of Medicine (Winston-Salem, North Carolina, USA)[84].

Statistical analysis

Sample size was determined according to power analysis. Animals were randomly assigned to treatment and control groups, and analysis was performed in a blinded fashion. After testing for normality (Bartlett's test), intergroup differences were analyzed by unpaired two-tailed t-test for single comparison, or by 1-way ANOVA or 2-way ANOVA with Tukey's or Bonferroni's multiple comparison test, as appropriate and indicated in the figure legends. If non-parametric testing was indicated, intergroup differences were analyzed by Mann-Whitney test or Kruskal-Wallis

test with Dunn's correction, as appropriate and indicated in the figure legends. Statistical tests through the manuscript were performed using Prism 7 (GraphPad).

ACKNOWLEDGEMENTS

This work was supported by grants R37-NS089323 (CI), R01-NS095441(CI) and K22-NS123507 (MMS), as well as the Leon Levy Fellowship in Neuroscience (MMS). The support from the Feil Family Foundation is gratefully acknowledged. The authors declare no competing financial interests.

REFERENCES

1. Levine DA, Springer MV, Brodtmann A. Blood pressure and vascular cognitive impairment. *Stroke*. 2022;53:1104-1113
2. Muntner P, Miles MA, Jaeger BC, Hannon L, 3rd, Hardy ST, Ostchega Y, et al. Blood pressure control among us adults, 2009 to 2012 through 2017 to 2020. *Hypertension*. 2022:101161hypertensionaha12219222
3. Carey RM, Sakhuja S, Calhoun DA, Whelton PK, Muntner P. Prevalence of apparent treatment-resistant hypertension in the united states. *Hypertension*. 2019;73:424-431
4. Williamson JD, Pajewski NM, Auchus AP, Bryan RN, Chelune G, Cheung AK, et al. Effect of intensive vs standard blood pressure control on probable dementia: A randomized clinical trial. *Jama*. 2019;321:553-561
5. Webb AJS, Werring DJ. New insights into cerebrovascular pathophysiology and hypertension. *Stroke*. 2022;53:1054-1064
6. Iadecola C, Gottesman RF. Neurovascular and cognitive dysfunction in hypertension: Epidemiology, pathobiology and treatment. *Circ Res*. 2019;124:1025-1044
7. Oh YS, Appel LJ, Galis ZS, Hafler DA, He J, Hernandez AL, et al. National heart, lung, and blood institute working group report on salt in human health and sickness: Building on the current scientific evidence. *Hypertension*. 2016;68:281-288
8. Elijovich F, Weinberger MH, Anderson CA, Appel LJ, Bursztyn M, Cook NR, et al. Salt sensitivity of blood pressure: A scientific statement from the american heart association. *Hypertension*. 2016;68:e7-e46
9. Grobe JL, Buehrer BA, Hilzendeger AM, Liu X, Davis DR, Xu D, et al. Angiotensinergic signaling in the brain mediates metabolic effects of deoxycorticosterone (doca)-salt in c57 mice. *Hypertension*. 2011;57:600-607
10. Basting T, Lazartigues E. Doca-salt hypertension: An update. *Curr Hypertens Rep*. 2017;19:32
11. Meade TW, Imeson JD, Gordon D, Peart WS. The epidemiology of plasma renin. *Clin Sci (Lond)*. 1983;64:273-280
12. Alderman MH, Madhavan S, Ooi WL, Cohen H, Sealey JE, Laragh JH. Association of the renin-sodium profile with the risk of myocardial infarction in patients with hypertension. *N Engl J Med*. 1991;324:1098-1104

13. Madhur MS, Lob HE, McCann LA, Iwakura Y, Blinder Y, Guzik TJ, et al. Interleukin 17 promotes angiotensin ii-induced hypertension and vascular dysfunction. *Hypertension*. 2010;55:500-507
14. Yao W, Sun Y, Wang X, Niu K. Elevated serum level of interleukin 17 in a population with prehypertension. *J Clin Hypertens (Greenwich)*. 2015;17:770-774
15. Simundic T, Jelakovic B, Dzumhur A, Turk T, Sahinovic I, Dobrosevic B, et al. Interleukin 17a and toll-like receptor 4 in patients with arterial hypertension. *Kidney Blood Press Res*. 2017;42:99-108
16. Itani HA, McMaster WG, Jr., Saleh MA, Nazarewicz RR, Mikolajczyk TP, Kaszuba AM, et al. Activation of human t cells in hypertension: Studies of humanized mice and hypertensive humans. *Hypertension*. 2016;68:123-132
17. Kim S, Goel R, Kumar A, Qi Y, Lobaton G, Hosaka K, et al. Imbalance of gut microbiome and intestinal epithelial barrier dysfunction in patients with high blood pressure. *Clin Sci (Lond)*. 2018;132:701-718
18. Kleinewietfeld M, Manzel A, Titze J, Kvakan H, Yosef N, Linker RA, et al. Sodium chloride drives autoimmune disease by the induction of pathogenic th17 cells. *Nature*. 2013;496:518-522
19. Wilck N, Matus MG, Kearney SM, Olesen SW, Forslund K, Bartolomaeus H, et al. Salt-responsive gut commensal modulates th17 axis and disease. *Nature*. 2017;551:585-589
20. Wu C, Yosef N, Thalhamer T, Zhu C, Xiao S, Kishi Y, et al. Induction of pathogenic th17 cells by inducible salt-sensing kinase sgk1. *Nature*. 2013;496:513-517
21. Faraco G, Park L, Anrather J, Iadecola C. Brain perivascular macrophages: Characterization and functional roles in health and disease. *J Mol Med (Berl)*. 2017;95:1143-1152
22. Kierdorf K, Masuda T, Jordao MJC, Prinz M. Macrophages at cns interfaces: Ontogeny and function in health and disease. *Nat Rev Neurosci*. 2019;20:547-562
23. Faraco G, Park L, Zhou P, Luo W, Paul SM, Anrather J, et al. Hypertension enhances abeta-induced neurovascular dysfunction, promotes beta-secretase activity, and leads to amyloidogenic processing of app. *J Cereb Blood Flow Metab*. 2016;36:241-252
24. Kopp C, Linz P, Dahlmann A, Hammon M, Jantsch J, Müller DN, et al. 23na magnetic resonance imaging-determined tissue sodium in healthy subjects and hypertensive patients. *Hypertension*. 2013;61:635-640
25. Faraco G, Sugiyama Y, Lane D, Garcia-Bonilla L, Chang H, Santisteban MM, et al. Perivascular macrophages mediate the neurovascular and cognitive dysfunction associated with hypertension. *J Clin Invest*. 2016;126:4674-4689
26. Faraco G, Brea D, Garcia-Bonilla L, Wang G, Racchumi G, Chang H, et al. Dietary salt promotes neurovascular and cognitive dysfunction through a gut-initiated th17 response. *Nat Neurosci*. 2018;21:240-249
27. Toda N, Ayajiki K, Okamura T. Cerebral blood flow regulation by nitric oxide: Recent advances. *Pharmacol Rev*. 2009;61:62-97
28. Esplugues E, Huber S, Gagliani N, Hauser AE, Town T, Wan YY, et al. Control of th17 cells occurs in the small intestine. *Nature*. 2011;475:514-518
29. Benakis C, Brea D, Caballero S, Faraco G, Moore J, Murphy M, et al. Commensal microbiota affects ischemic stroke outcome by regulating intestinal gammadelta t cells. *Nat Med*. 2016;22:516-523
30. Korbelin J, Dogbevia G, Michelfelder S, Ridder DA, Hunger A, Wenzel J, et al. A brain microvasculature endothelial cell-specific viral vector with the potential to treat neurovascular and neurological diseases. *EMBO Mol Med*. 2016;8:609-625
31. Santisteban MM, Ahn SJ, Lane D, Faraco G, Garcia-Bonilla L, Racchumi G, et al. Endothelium-macrophage crosstalk mediates blood-brain barrier dysfunction in hypertension. *Hypertension*. 2020;76:795-807

32. El Malki K, Karbach SH, Huppert J, Zayoud M, Reissig S, Schuler R, et al. An alternative pathway of imiquimod-induced psoriasis-like skin inflammation in the absence of interleukin-17 receptor a signaling. *J Invest Dermatol*. 2013;133:441-451
33. Nikolakopoulou AM, Wang Y, Ma Q, Sagare AP, Montagne A, Huuskonen MT, et al. Endothelial lrp1 protects against neurodegeneration by blocking cyclophilin a. *J Exp Med*. 2021;218
34. Van Hove H, Martens L, Scheyltjens I, De Vlaminck K, Pombo Antunes AR, De Prijck S, et al. A single-cell atlas of mouse brain macrophages reveals unique transcriptional identities shaped by ontogeny and tissue environment. *Nat Neurosci*. 2019;22:1021-1035
35. Park L, Uekawa K, Garcia-Bonilla L, Koizumi K, Murphy M, Pistik R, et al. Brain perivascular macrophages initiate the neurovascular dysfunction of alzheimer abeta peptides. *Circ Res*. 2017;121:258-269
36. Polfliet MM, Goede PH, van Kesteren-Hendrikx EM, van Rooijen N, Dijkstra CD, van den Berg TK. A method for the selective depletion of perivascular and meningeal macrophages in the central nervous system. *J Neuroimmunol*. 2001;116:188-195
37. Sayd A, Vargas-Caraveo A, Perea-Romero I, Robledo-Montaña J, Caso JR, Madrigal JLM, et al. Depletion of brain perivascular macrophages regulates acute restraint stress-induced neuroinflammation and oxidative/nitrosative stress in rat frontal cortex. *Eur Neuropsychopharmacol*. 2020;34:50-64
38. Mendiola AS, Ryu JK, Bardehle S, Meyer-Franke A, Ang KK, Wilson C, et al. Transcriptional profiling and therapeutic targeting of oxidative stress in neuroinflammation. *Nat Immunol*. 2020;21:513-524
39. Ivan DC, Walthert S, Berve K, Steudler J, Locatelli G. Dwellers and trespassers: Mononuclear phagocytes at the borders of the central nervous system. *Front Immunol*. 2020;11:609921
40. Garcia-Bonilla L, Sciortino R, Shahanoor Z, Racchumi G, Janakiraman M, Montaner J, et al. Role of microglial and endothelial cd36 in post-ischemic inflammasome activation and interleukin-1β-induced endothelial activation. *Brain Behav Immun*. 2021;95:489-501
41. Hohsfield LA, Najafi AR, Ghorbanian Y, Soni N, Hingco EE, Kim SJ, et al. Effects of long-term and brain-wide colonization of peripheral bone marrow-derived myeloid cells in the cns. *J Neuroinflammation*. 2020;17:279
42. Chinnery HR, Ruitenberg MJ, McMenamin PG. Novel characterization of monocyte-derived cell populations in the meninges and choroid plexus and their rates of replenishment in bone marrow chimeric mice. *J Neuropathol Exp Neurol*. 2010;69:896-909
43. Louveau A, Herz J, Alme MN, Salvador AF, Dong MQ, Viar KE, et al. Cns lymphatic drainage and neuroinflammation are regulated by meningeal lymphatic vasculature. *Nat Neurosci*. 2018;21:1380-1391
44. Rua R, McGavern DB. Advances in meningeal immunity. *Trends Mol Med*. 2018;24:542-559
45. Alves de Lima K, Rustenhoven J, Da Mesquita S, Wall M, Salvador AF, Smirnov I, et al. Meningeal γδ t cells regulate anxiety-like behavior via il-17a signaling in neurons. *Nat Immunol*. 2020
46. Ribeiro M, Brigas HC, Temido-Ferreira M, Pousinha PA, Regen T, Santa C, et al. Meningeal γδ t cell-derived il-17 controls synaptic plasticity and short-term memory. *Sci Immunol*. 2019;4
47. Rustenhoven J, Drieu A, Mamuladze T, de Lima KA, Dykstra T, Wall M, et al. Functional characterization of the dural sinuses as a neuroimmune interface. *Cell*. 2021;184:1000-1016.e1027

48. Ranieri E, Netti GS, Gigante M. Ctl elispot assay and t cell detection. *Methods Mol Biol*. 2021;2325:65-77
49. Prinz I, Silva-Santos B, Pennington DJ. Functional development of γδ t cells. *Eur J Immunol*. 2013;43:1988-1994
50. Gray EE, Ramírez-Valle F, Xu Y, Wu S, Wu Z, Karjalainen KE, et al. Deficiency in il-17-committed vγ4(+) γδ t cells in a spontaneous sox13-mutant cd45.1(+) congenic mouse substrain provides protection from dermatitis. *Nat Immunol*. 2013;14:584-592
51. McKenzie DR, Kara EE, Bastow CR, Tyllis TS, Fenix KA, Gregor CE, et al. Il-17-producing γδ t cells switch migratory patterns between resting and activated states. *Nat Commun*. 2017;8:15632
52. Maeda Y, Seki N, Kataoka H, Takemoto K, Utsumi H, Fukunari A, et al. Il-17-producing vγ4+ γδ t cells require sphingosine 1-phosphate receptor 1 for their egress from the lymph nodes under homeostatic and inflammatory conditions. *J Immunol*. 2015;195:1408-1416
53. Mandala S, Hajdu R, Bergstrom J, Quackenbush E, Xie J, Milligan J, et al. Alteration of lymphocyte trafficking by sphingosine-1-phosphate receptor agonists. *Science*. 2002;296:346-349
54. Chiba K, Yanagawa Y, Masubuchi Y, Kataoka H, Kawaguchi T, Ohtsuki M, et al. Fty720, a novel immunosuppressant, induces sequestration of circulating mature lymphocytes by acceleration of lymphocyte homing in rats. *J Immunol*. 1998;160:5037-5044
55. Enosawa S, Suzuki S, Kakefuda T, Li XK, Amemiya H. Induction of selective cell death targeting on mature t-lymphocytes in rats by a novel immunosuppressant, fty720. *Immunopharmacology*. 1996;34:171-179
56. De Silva TM, Modrick ML, Grobe JL, Faraci FM. Activation of the central renin-angiotensin system causes local cerebrovascular dysfunction. *Stroke*. 2021;52:2404-2413
57. Lu X, Crowley SD. The immune system in hypertension: A lost shaker of salt 2021 lewis k. Dahl memorial lecture. *Hypertension*. 2022;79:1339-1347
58. Guzik TJ, Hoch NE, Brown KA, McCann LA, Rahman A, Dikalov S, et al. Role of the t cell in the genesis of angiotensin ii induced hypertension and vascular dysfunction. *J Exp Med*. 2007;204:2449-2460
59. Norlander AE, Madhur MS, Harrison DG. The immunology of hypertension. *J Exp Med*. 2018;215:21-33
60. Drummond GR, Vinh A, Guzik TJ, Sobey CG. Immune mechanisms of hypertension. *Nat Rev Immunol*. 2019;19:517-532
61. Higaki A, Mahmoud AUM, Paradis P, Schiffrin EL. Role of interleukin-23/interleukin-17 axis in t-cell mediated actions in hypertension. *Cardiovasc Res*. 2020;117:1274-1283
62. Lerman LO, Kurtz TW, Touyz RM, Ellison DH, Chade AR, Crowley SD, et al. Animal models of hypertension: A scientific statement from the american heart association. *Hypertension*. 2019:e87-e120
63. Gorelick PB, Scuteri A, Black SE, Decarli C, Greenberg SM, Iadecola C, et al. Vascular contributions to cognitive impairment and dementia: A statement for healthcare professionals from the american heart association/american stroke association. *Stroke*. 2011;42:2672-2713
64. Cortes-Canteli M, Iadecola C. Alzheimer's disease and vascular aging: Jacc focus seminar. *J Am Coll Cardiol*. 2020;75:942-951
65. Brigas HC, Ribeiro M, Coelho JE, Gomes R, Gomez-Murcia V, Carvalho K, et al. Il-17 triggers the onset of cognitive and synaptic deficits in early stages of alzheimer's disease. *Cell Rep*. 2021;36:109574
66. Salvador AF, de Lima KA, Kipnis J. Neuromodulation by the immune system: A focus on cytokines. *Nat Rev Immunol*. 2021;21:526-541

67. Rouch L, Cestac P, Hanon O, Cool C, Helmer C, Bouhanick B, et al. Antihypertensive drugs, prevention of cognitive decline and dementia: A systematic review of observational studies, randomized controlled trials and meta-analyses, with discussion of potential mechanisms. *CNS Drugs*. 2015;29:113-130
68. Ding J, Davis-Plourde KL, Sedaghat S, Tully PJ, Wang W, Phillips C, et al. Antihypertensive medications and risk for incident dementia and alzheimer's disease: A meta-analysis of individual participant data from prospective cohort studies. *Lancet Neurol*. 2020;19:61-70
69. James PA, Oparil S, Carter BL, Cushman WC, Dennison-Himmelfarb C, Handler J, et al. 2014 evidence-based guideline for the management of high blood pressure in adults: Report from the panel members appointed to the eighth joint national committee (jnc 8). *Jama*. 2014;311:507-520
70. Harrison DG, Coffman TM, Wilcox CS. Pathophysiology of hypertension: The mosaic theory and beyond. *Circ Res*. 2021;128:847-863
71. Ridker PM, Everett BM, Thuren T, MacFadyen JG, Chang WH, Ballantyne C, et al. Antiinflammatory therapy with canakinumab for atherosclerotic disease. *N Engl J Med*. 2017;377:1119-1131
72. Ma T, Wang F, Xu S, Huang JH. Meningeal immunity: Structure, function and a potential therapeutic target of neurodegenerative diseases. *Brain Behav Immun*. 2021;93:264-276
73. Hayashi S, Lewis P, Pevny L, McMahon AP. Efficient gene modulation in mouse epiblast using a sox2cre transgenic mouse strain. *Mech Dev*. 2002;119 Suppl 1:S97-s101
74. Belanger KM, Crislip GR, Gillis EE, Abdelbary M, Musall JB, Mohamed R, et al. Greater t regulatory cells in females attenuate doca-salt-induced increases in blood pressure versus males. *Hypertension*. 2020;75:1615-1623
75. Korvela M, Lind AL, Wetterhall M, Gordh T, Andersson M, Pettersson J. Quantification of 10 elements in human cerebrospinal fluid from chronic pain patients with and without spinal cord stimulation. *J Trace Elem Med Biol*. 2016;37:1-7
76. Bischoff K, Lamm C, Erb HN, Hillebrandt JR. The effects of formalin fixation and tissue embedding of bovine liver on copper, iron, and zinc analysis. *J Vet Diagn Invest*. 2008;20:220-224
77. Capone C, Faraco G, Park L, Cao X, Davisson RL, Iadecola C. The cerebrovascular dysfunction induced by slow pressor doses of angiotensin ii precedes the development of hypertension. *Am J Physiol Heart Circ Physiol*. 2011;300:H397-407
78. Kazama K, Wang G, Frys K, Anrather J, Iadecola C. Angiotensin ii attenuates functional hyperemia in the mouse somatosensory cortex. *Am J Physiol Heart Circ Physiol*. 2003;285:H1890-1899
79. Kober F, Iltis I, Izquierdo M, Desrois M, Ibarrola D, Cozzone PJ, et al. High-resolution myocardial perfusion mapping in small animals in vivo by spin-labeling gradient-echo imaging. *Magn Reson Med*. 2004;51:62-67
80. Deacon RM. Assessing nest building in mice. *Nat Protoc*. 2006;1:1117-1119
81. Faraco G, Hochrainer K, Segarra SG, Schaeffer S, Santisteban MM, Menon A, et al. Dietary salt promotes cognitive impairment through tau phosphorylation. *Nature*. 2019;574:686-690
82. Louveau A, Filiano A, Kipnis J. Meningeal whole mount preparation and characterization of neural cells by flow cytometry. *Curr Protoc Immunol*. 2018;121
83. Park L, Wang G, Zhou P, Zhou J, Pitstick R, Previti ML, et al. Scavenger receptor cd36 is essential for the cerebrovascular oxidative stress and neurovascular dysfunction induced by amyloid-beta. *Proc Natl Acad Sci U S A*. 2011;108:5063-5068
84. Nakamoto H, Ferrario CM, Fuller SB, Robaczewski DL, Winicov E, Dean RH. Angiotensin-(1-7) and nitric oxide interaction in renovascular hypertension. *Hypertension*. 1995;25:796-802

1

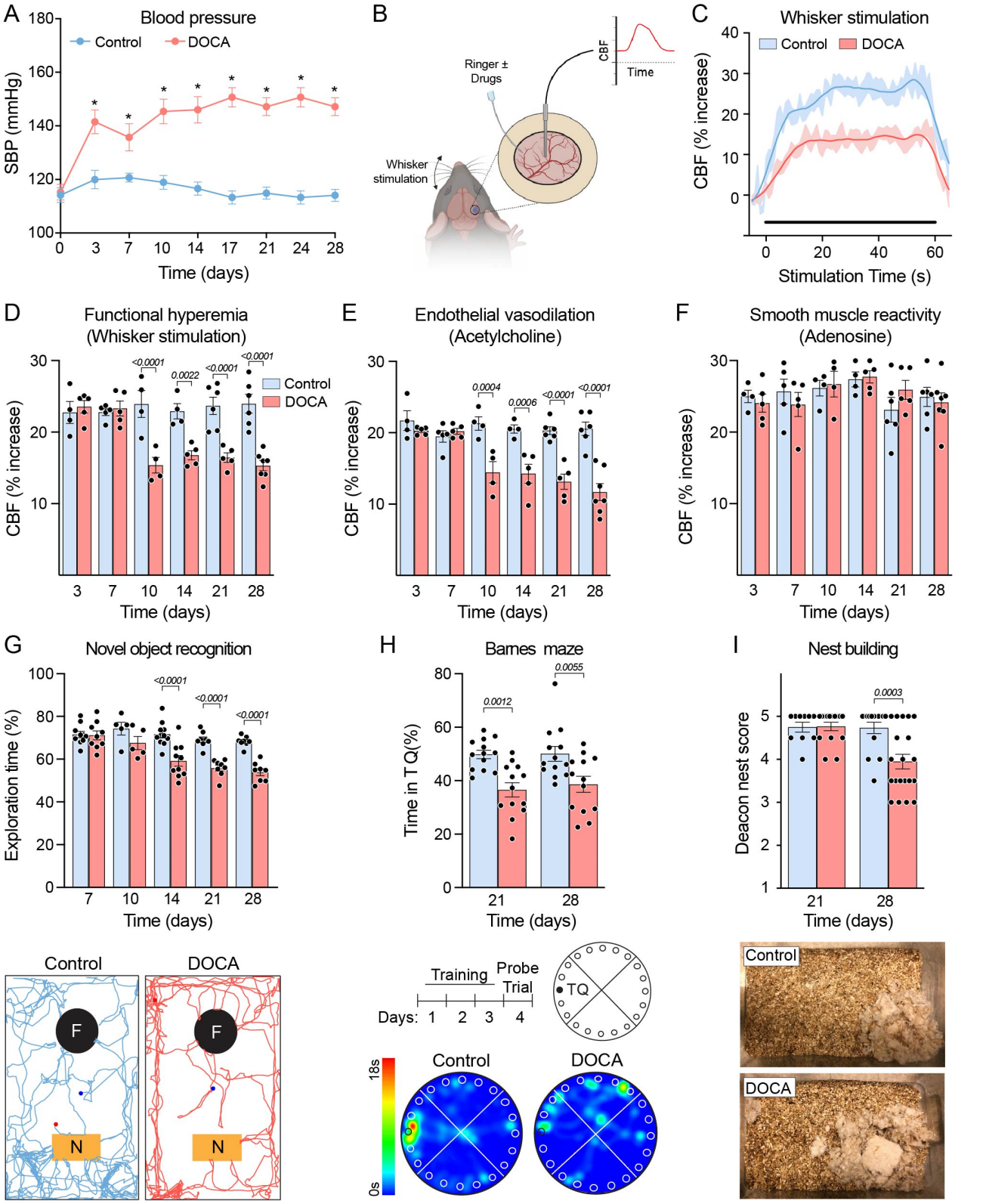

Figure 1. DOCA-salt hypertension induces neurovascular and cognitive impairment. (A) Systolic blood pressure (SBP), assessed by tail cuff plethysmography, is elevated in DOCA-salt hypertension over 28 days of treatment (HTN: p<0.0001, time: p<0.0001, interaction: p<0.0001; n=15). **(B)** Schematic of methods used to assess neurovascular function. **(C-D)** DOCA attenuates the increase in cerebral blood flow (CBF) induced by 60s stimulation of the facial whiskers (functional hyperemia),

beginning at 10 days of DOCA (HTN: $p<0.0001$, time: $p=0.001$, interaction: $p<0.0001$; n=4-7). **(E)** Endothelial vasodilation was attenuated by DOCA beginning at 10 days (HTN: $p<0.0001$, time: $p<0.0001$, interaction: $p<0.0001$; n=4-7). **(F)** No difference was observed in smooth muscle reactivity (HTN: $p=0.9702$, time: $p=.1981$, interaction: $p=.6479$; n=4-7). **(G-I)** DOCA induced cognitive impairment assessed by **(G)** percent time exploring a novel object (HTN: $p<0.0001$, time: $p<0.0001$, interaction: 0.0012; n=5-11), **(H)** time in target quadrant (TQ) during Barnes maze probe trial (HTN: $p<0.0001$, time: $p=0.6531$, interaction: 0.7123; n=13), and **(I)** nest building assessed on the Deacon score scale (HTN: $p=0.0125$, time: $p=0.0069$, interaction: p=0093; n=10-20). All intergroup differences analyzed by two-way ANOVA and Bonferroni's multiple comparison test.

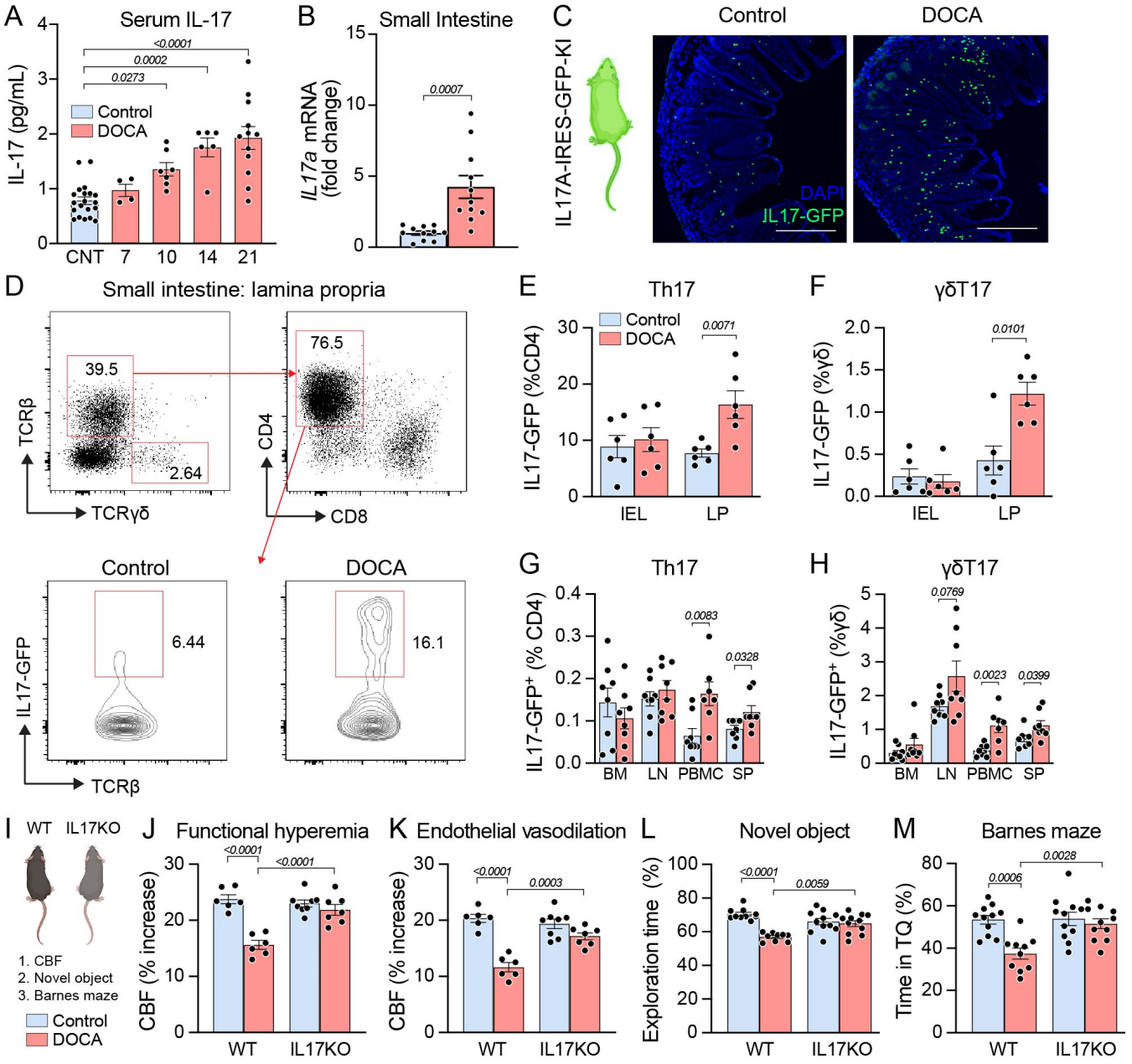

Figure 2. The neurovascular and cognitive impairment induced by DOCA is mediated by IL-17. **(A)** Serum IL-17 is elevated in DOCA HTN starting at 10 days ($p<0.0001$; one-way ANOVA and Bonferroni's multiple comparison test; n=5-18 as shown). **(B)** DOCA increased *Il17a* mRNA (unpaired two-tailed t-test, n=11) as well as **(C)** IL17-GFP cells in the small intestine. **(D)** By flow cytometry, these cells were identified to be **(E)** Th17 and **(F)** γδT17 in the lamina propria (LP) not intraepithelial lymphocytes (IEL) (unpaired two-tailed t-test, n=6). **(G-H)** Th17 and γδT17 were also expanded in peripheral blood mononuclear cells (PBMC) and spleen (SP), but not in the bone marrow (BM) or lymph nodes (LN) (unpaired two-tailed t-test per organ, n=7-8). **(I-M)** IL-17 deficient mice (KO) did not exhibit an attenuation in functional hyperemia (HTN: $p<0.0001$, genotype: $p=0.0024$, interaction: $p=0.0002$; two-way ANOVA and Bonferroni's multiple comparison test; n=6-8) and endothelial vasodilation (HTN: $p<0.0001$, genotype: $p=0.0079$, interaction: $p=0.0004$; two-way ANOVA and Bonferroni's multiple comparison test; n=6-8), and no deficits were observed in either novel object (HTN: $p<0.0001$, genotype: $p=2603$, interaction: $p=0.0003$; two-way ANOVA and Bonferroni's multiple comparison test; n=9-11) or Barnes maze tests (HTN: $p=0.001$, genotype: $p=0.0076$, interaction: $p=0.0114$; two-way ANOVA and Bonferroni's multiple comparison test; n=9-11).

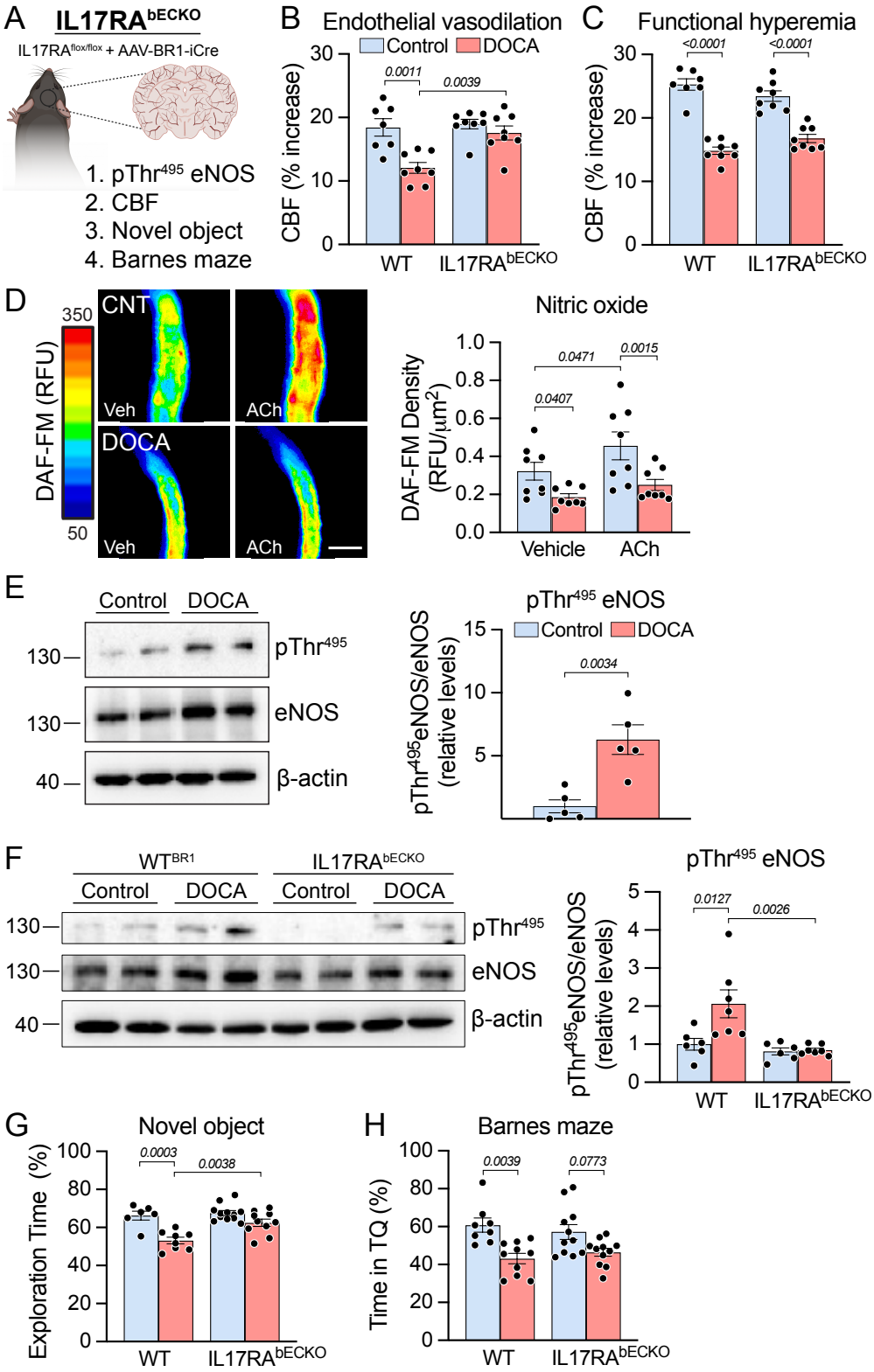

Figure 3. IL-17 impairs endothelial vasodilation by downregulating NO bioavailability via endothelial IL-17 receptors. (A-C) IL17RA brain endothelial cell knockout (IL17RAb^{ECKO}) mice are protected from the impairment in endothelial vasodilation (HTN: p=0.0007, genotype: p=0.0067, interaction: p=0.0223; two-way ANOVA and Bonferroni's multiple comparison test; n=7-8) but not the impairment in functional hyperemia induced by DOCA (HTN: p<0.0001, genotype: p=0.9446, interaction: p=0.0161; two-way ANOVA and Bonferroni's multiple comparison test; n=7-8). **(D)** Resting and ACh-induced endothelial NO production was attenuated in DOCA cerebral microvascular

preparations ($p<0.0001$, repeated measured one-way ANOVA and Tukey's multiple comparison test; n=8). **(E-F)** eNOS inhibitory phosphorylation was increased by DOCA in WT mice (unpaired two-tailed t-test), an effect suppressed in IL-17RAb^{ECKO} (HTN: $p=0.0185$, genotype: $p=0.0037$, interaction: $p=0.0266$; two-way ANOVA and Bonferroni's multiple comparison test; n=5-7). **(G-H)** IL17RAb^{ECKO} displayed cognitive improvement only at novel object recognition (HTN: $p<0.0001$, genotype: $p=0.0061$, interaction: $p=0.0338$; two-way ANOVA and Tukey's multiple comparison test; n=6-12), not the Barnes maze (HTN: $p<0.0001$, genotype: $p=0.9599$, interaction: $p=0.2875$; two-way ANOVA and Tukey's multiple comparison test; n=6-12).

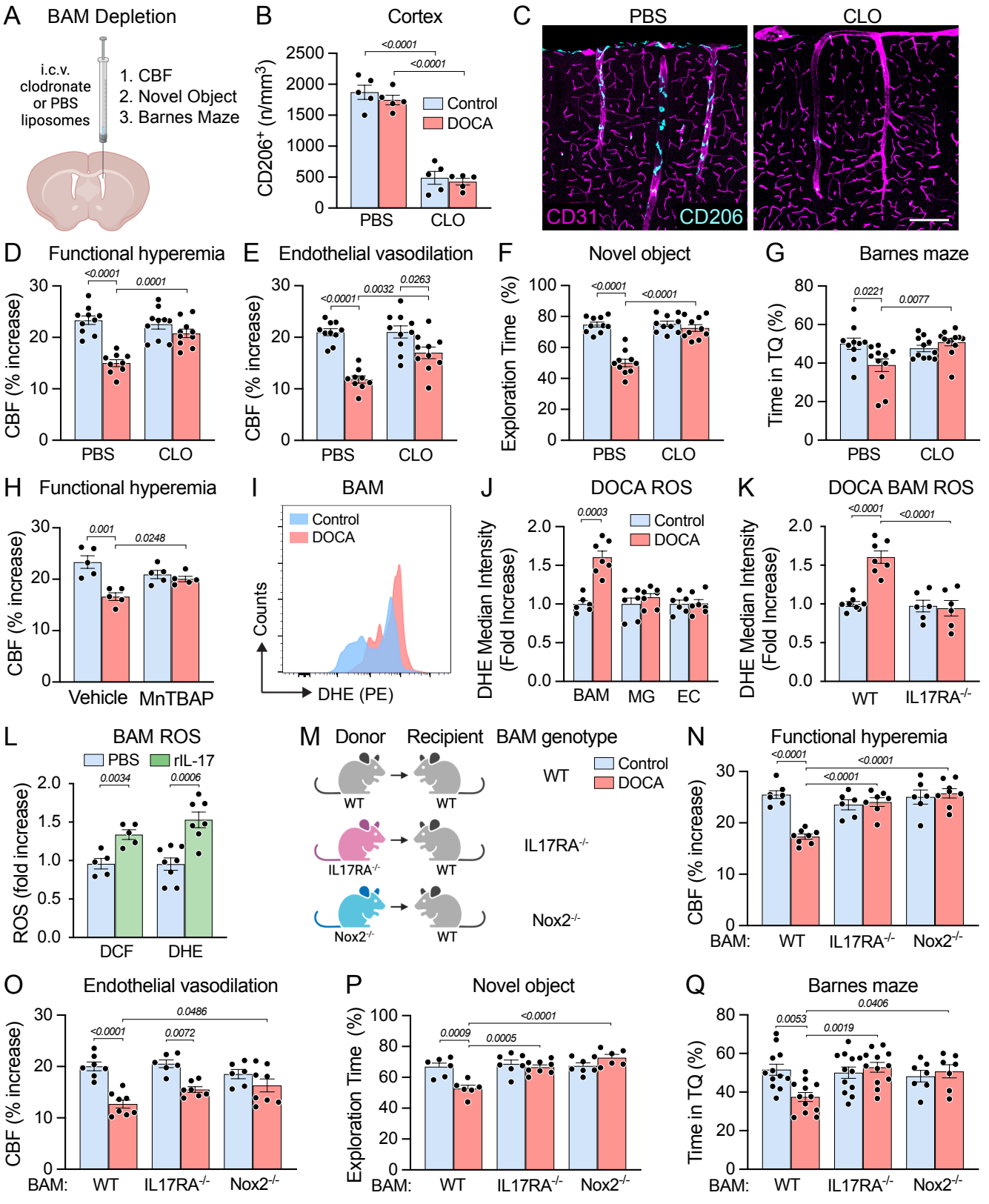

Figure 4. IL-17 impairs functional hyperemia via enhanced free radical production mediated by IL-17RA in BAM. (A-C) Brain associated macrophage (BAM), including perivascular and leptomeningeal macrophages, were depleted by 80% 21 days after intracerebroventricular delivery of liposome-encapsulated clodronate depletes (HTN: p=0.3156, liposomes: p=<0.0001, interaction: p=0.7304; two-way ANOVA and Tukey's multiple comparison test; n=5). **(D-G)** BAM depletion

normalized functional hyperemia (HTN: p<0.0001, liposomes: p=0.0050, interaction: p=0.0004; two-way ANOVA and Tukey's multiple comparison test; n=9-10) and partially improved endothelial vasoactivity (HTN: p<0.0001, liposomes: p=0.01, interaction: p=0.0112, two-way ANOVA and Tukey's multiple comparison test; n=9-10) while also improving cognitive function assessed by novel object recognition (HTN: p<0.0001, liposomes: p<0.0001, interaction: p<0.0001, two-way ANOVA and Bonferroni's multiple comparison test; n=10) and Barnes maze (HTN: p=0.1240, liposomes: p=0.0648, interaction: p=0.0062, two-way ANOVA and Bonferroni's multiple comparison test; n=10-12). **(H)** Neocortical application of the ROS scavenger MnTBAP rescued the impairment of functional hyperemia in DOCA-salt (p=0.0017, repeated measures one-way ANOVA with Tukey's multiple comparison test, n=5). **(I-K)** The increased ROS production in BAM induced by DOCA-salt (HTN: p=0.0033, cell type: p<0.0001, interaction: p<0.0001; two-way repeated measures ANOVA with Bonferroni's multiple comparisons test; n=6-7) is prevented in IL-17RA deficient mice (HTN: p=0.0006, genotype: p<0.0001, interaction: p=0.0002; two-way ANOVA with Bonferroni's multiple comparison test; n=6-8). **(L)** Recombinant IL-17 increased ROS production in BAM (unpaired two-tailed t-test per ROS indicator, n=5-8). **(M-Q)** Deletion of either IL-17RA or Nox2 from BAM in BM chimeras prevented the impairment of functional hyperemia in full (HTN: p=0.0030, BAM genotype: p=0.0003, interaction: p<0.0001; two-way ANOVA with Tukey's multiple comparison test; n=6-8), improved endothelial vasoactivity (HTN: p<0.0001, BAM genotype: p=0.1898, interaction: p=0.0248; two-way ANOVA with Tukey's multiple comparison test; n=6-8), as well as cognitive function (novel object HTN: p=0.0392, BAM genotype: p<0.0001; interaction: p=0.0004; Barnes HTN: p=0.2287, BAM genotype: p=0.0362, interaction: p=0.0040; two-way ANOVA with Tukey's multiple comparison test; n=6-8).

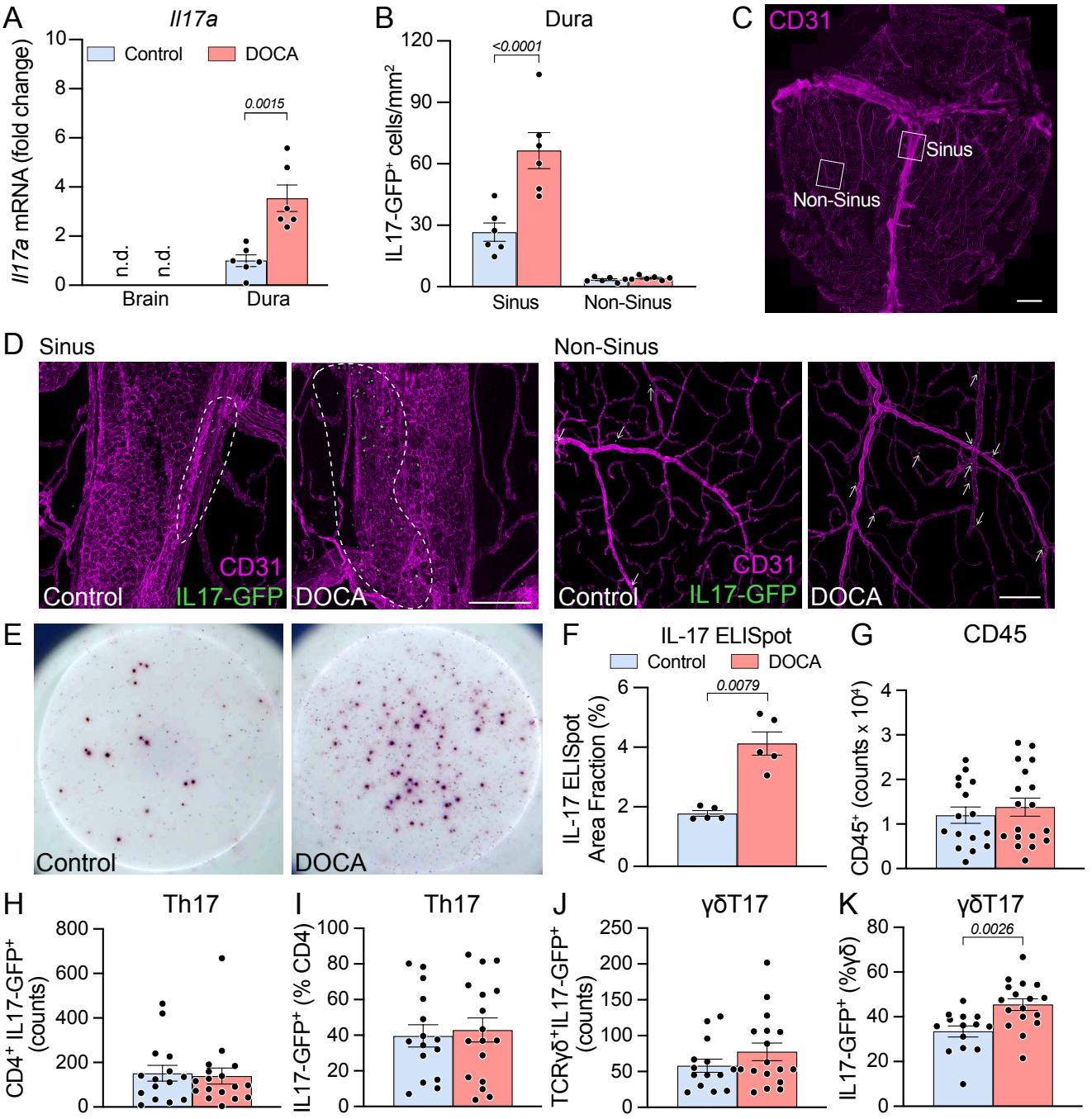

Figure 5. Salt-sensitive hypertension increases IL17-producing T cells in the dura mater. (A) *Il17a* mRNA was not observed in the brain parenchyma, but it was detected in stripped meninges of control mice and was markedly increased by DOCA-salt (unpaired two-tailed t-test; n=6). **(B-D)** DOCA-salt treatment led to a significant increase in IL17-GFP+ cells in the vicinity of the venous sinuses (two-way repeated measures ANOVA with Bonferroni's multiple comparison test; HTN: p=0.0017, Sinus: p<0.0001, interaction: p=0.0034; n=6). **(E-F)** Dura mater cells secrete IL-17, and this response is increased in DOCA-salt mice (unpaired two-tailed t-test; n=5). **(G-K)** DOCA-salt increases the percentage of γδT17 cells but no difference in Th17 cells (unpaired two-tailed t-test; n=14-17).

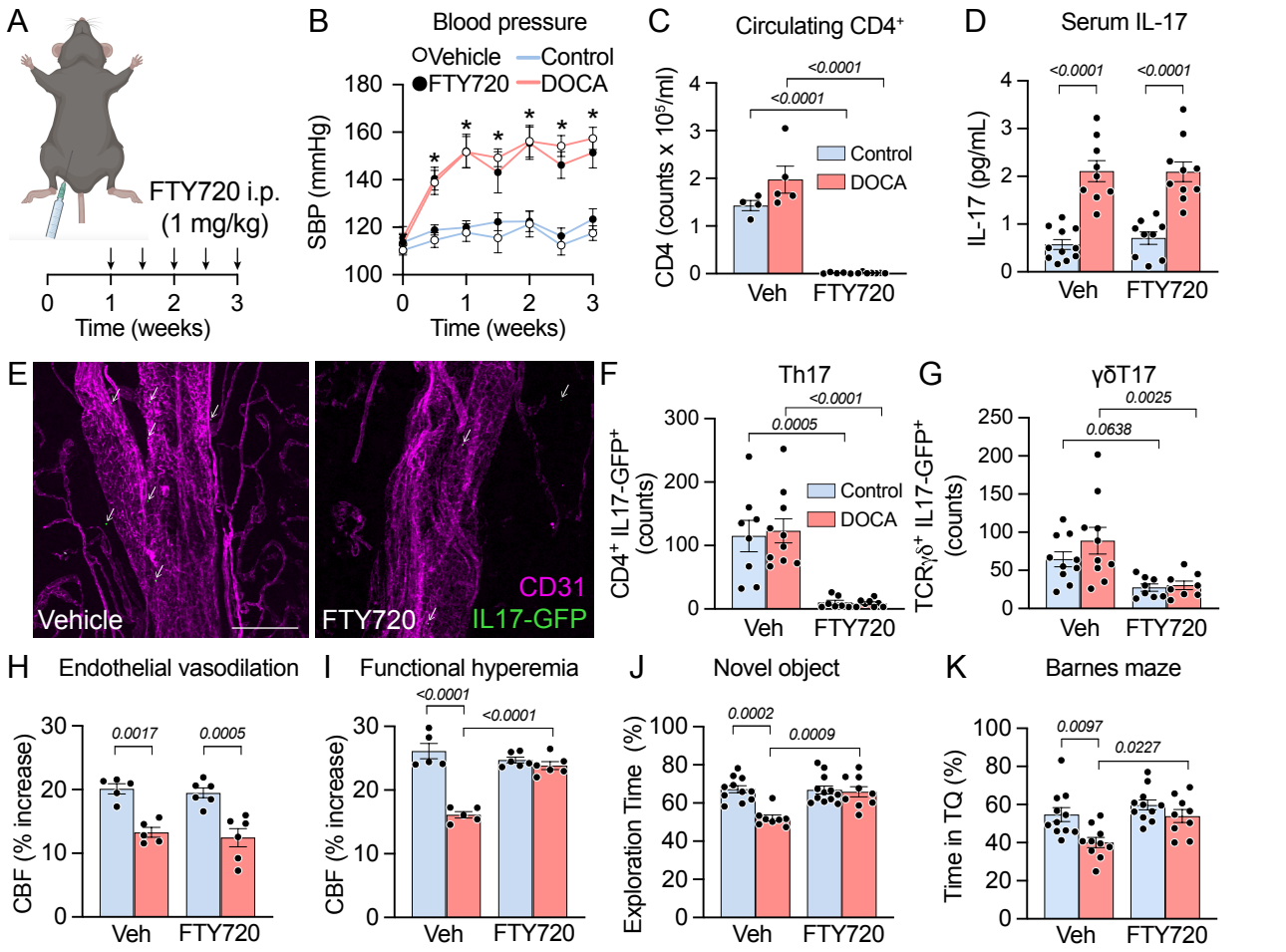

Figure 6. Cognitive impairment in salt-sensitive hypertension is driven by meningeal IL17-producing T cells. (A-B) FTY720 was administered from day 7 through day 21 of DOCA-salt and did not affect the increase in systolic blood pressure (treatment: p<0.0001, time: p<0.0001, interaction: p=0.0182; two-way repeated measures ANOVA with Tukey's multiple comparison test; n=5-8). **(C-D)** FTY720 reduces circulating CD4 T cells (HTN: p=0.0705, treatment: p<0.0001, interaction: p=0.0737; two-way ANOVA with Tukey's multiple comparison test; n=4-7), without affecting the elevation in serum IL-17 in DOCA-salt (HTN: p<0.0001, treatment: p=0.7200, interaction: p=0.6622; two way ANOVA with Tukey's multiple comparison test; n=9-11). **(E-G)** FTY720 reduced IL17-GFP cells in the meninges, including both Th17 (HTN: p=0.8358, treatment: p<0.0001, interaction: p=0.7848; two-way ANOVA with Bonferroni's multiple comparison test; n=8-10) and γδT17 (HTN: p=0.2517, treatment: p=0.0003, interaction: p=0.3639; two-way ANOVA with Bonferroni's multiple comparison test; n=8-10). **(H-K)** FTY did not improve endothelial vasoactivity (HTN: p<0.0001, treatment: p=0.4839, interaction: p=0.9293; two-way ANOVA with Bonferroni's multiple comparison test; n=5-6), but completely restored functional hyperemia (HTN: p<0.0001, treatment: p=0.0004, interaction: p<0.0001; two-way ANOVA with Bonferroni's multiple comparison test; n=5-6), as well as improved cognitive function (novel object HTN: p=0.0007, treatment: p=0.0037; interaction: p=0.0023; Barnes HTN: p=0.0023, treatment: p=0.0045, interaction: p=0.1695; two-way ANOVA with Tukey's multiple comparison test; n=8-12).

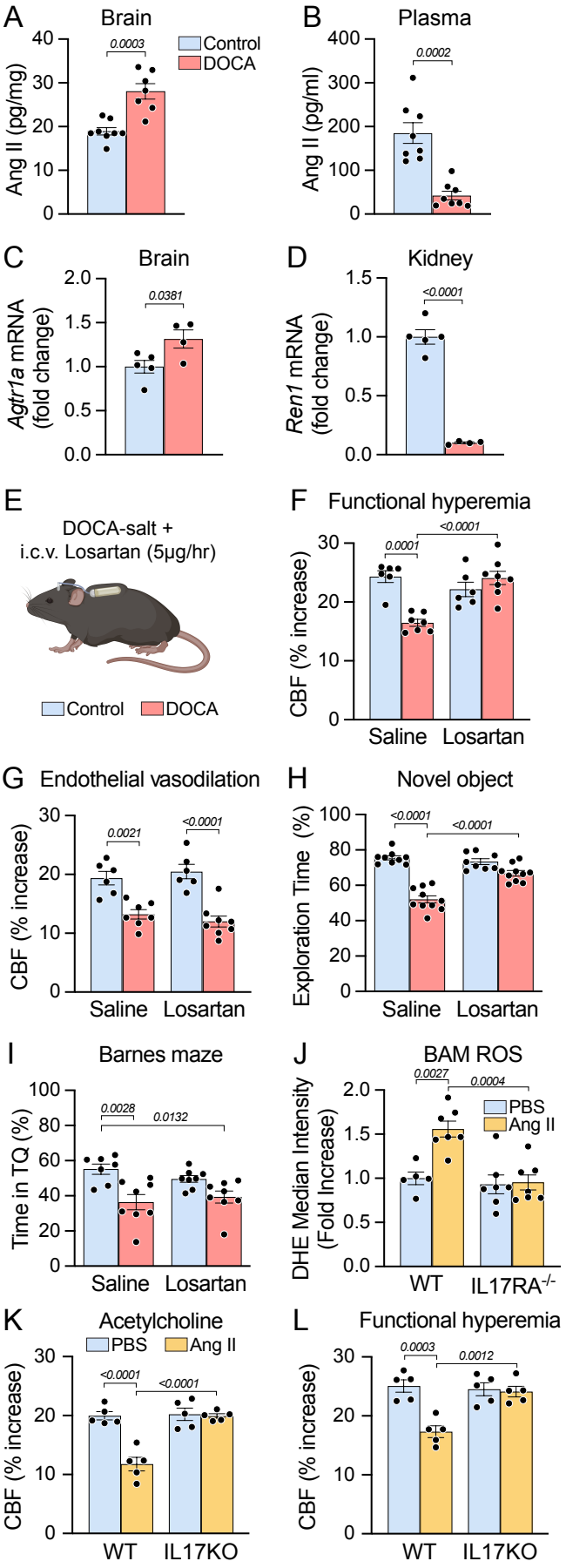

Figure 7. The contribution of Ang II to the cerebrovascular dysfunction in DOCA-salt depends on IL-17 signaling. (A-B) DOCA-salt treatment elevated Ang II levels in brain and reduced it in the circulation (unpaired two-tailed t-test; n=7-8). **(C-D)** DOCA-salt upregulates brain *Agtr1a* and downregulates kidney renin (unpaired two-tailed t-test; n=4-5). **(E-G)** Central AT1R blockade with i.c.v. losartan restored functional hyperemia (HTN: p=0.0088, treatment: p=0.0148, interaction: p<0.0001; two-way ANOVA with Bonferroni's multiple comparison test; n=6-8), but did not improve endothelium-dependent vasodilation (HTN: p<0.0001, treatment: p=0.9604, interaction: p=0.2642; two-way ANOVA with Bonferroni's multiple comparison test; n=6-8). **(H-I)** Central AT1R blockade improved novel object recognition (HTN: p<0.0001, treatment: p=0.0005, interaction: p<0.0001; two-way ANOVA with Tukey's multiple comparison test; n=8-10), but did not improve Barnes maze (HTN: p=0.0002; treatment: p=0.6968, interaction: p=0.2113; two-way ANOVA with Tukey's multiple comparison test; n=7-8). **(J)** Ang II stimulation increased ROS production in WT but not IL17RA$^{-/-}$ BAM (genotype: p=0.0015; treatment: p=0.0050, interaction: p=0.0087; two-way ANOVA with Tukey's multiple comparison test; n=5-7). **(K-L)** Neocortical application of Ang II impaired endothelial vasoactivity (genotype: p=0.0029; treatment: p=0.0003, interaction: p=0.0004; two-way repeated measures ANOVA with Bonferroni's multiple comparison test; n=5) and induced neurovascular dysfunction (genotype: p=0.0374; treatment: p=0.0003, interaction: p=0.0005; two-way repeated measures ANOVA with Bonferroni's multiple comparison test; n=5) in WT but not IL17KO mice.